International Journal of Bifurcation and Chaos, Vol. 32, No. 13 (2022) 2250203 (35 pages)

DOI: 10.1142/S0218127422502030

Complex Dynamics of Predator–Prey Systems with Allee Effect

Yanni Zeng* and Pei Yu†
Department of Applied Mathematics, Western University,
London, Ontario, Canada N6A 5B7
**yzeng243@uwo.ca*
†pyu@uwo.ca

Received August 8, 2022; Revised August 26, 2022

In this paper, we apply bifurcation theory to consider four predator–prey systems which include the Allee effect, and show that the species having a strong Allee effct may affect their predation and hence extinction risk. It is shown that the models with the Allee effect exhibit more complex dynamical behaviors compared with that without the Allee effect. In particular, two models with no Allee effect do not have Hopf bifurcation, but can have Hopf bifurcation with the Allee effect; and one model, which does not have Bogdanov–Takens bifurcation if no Allee effect is involved, can have Bogdanov–Takens bifurcation of codimension two. Especially, for one model with Holling type II functional response of the predator to the prey, the Allee effect not only completely changes the stability of the equilibrium at the origin, but also changes the supercritical Hopf bifurcation arising from an interior equilibrium to subcritical Hopf bifurcation with very limited parameter values to yield unstable limit cycles, and further increases the system's stability.

Keywords: Predator–prey system; Allee effect; Hopf bifurcation; Bogdanov–Takens bifurcation; normal form; the simplest normal form; limit cycle.

1. Introduction

The dynamics of a population is greatly affected by its interaction with other populations. There exist many kinds of interaction among populations, such as competition, predation, parasitism and mutualism. The predator–prey interaction is one of the most fundamental interactions and one of the most fascinating interactions to investigate. A lot of attention has been paid by many researchers to model these various kinds of interactions. Since the first predator–prey model was independently proposed by Lotka [1925] and Volterra [1926], the construction of the predator–prey models and the study on the population dynamics have remained a dominant branch in theoretical and mathematical ecology (e.g. see [Freedman, 1980; Murray, 2002] and references therein). After this pioneering work of Lotka and Volterra, predator–prey models with different kinds of prey-dependent functional response were studied extensively [Arditi & Ginzburg, 1989; Holling, 1959; Huang *et al.*, 2014; Murray, 2002]. A well-known generalized Gause predator–prey model [Freedman, 1980; Gause, 1969] is described by

$$\begin{aligned}\dot{x} &= rx\left(1-\frac{x}{K}\right)-yp(\cdot),\\ \dot{y} &= y[cq(\cdot)-d],\end{aligned}\tag{1}$$

where dot denotes differentiation with respect to time t, x and y represent the population densities of

†Author for correspondence

prey and predator, respectively. The logistic growth function $rx(1-\frac{x}{K})$ is a typical function to describe the specific growth rate of the prey in the absence of predators, where the positive parameters r and K stand respectively for the prey's intrinsic growth rate and the carrying capacity of the prey. The positive parameters c and d denote the conversion rate of the prey to the predator and the predator death rate, respectively. $p(\cdot)$ is a functional response function, which reflects the capture ability of the predator to the prey, and $q(\cdot)$ describes how predator converts the consumed prey into the growth of predators. There are a lot of models developed using different functions p and q. Functional response is the key component in the predator–prey relationship, characterizing the rate of prey consumption by an average predator.

In prey-dependent functional response, the consumption rate is the function of prey density only, denoted by $p(x)$. However, later a lot of observations indicate that on large temporal and spatial scales, the predator may appear to search, compete or share for food and thus the functional response should depend on both the prey and predator. For example, in the case of perfect sharing, the predator-dependent functional response takes the ratio-dependent form in which functional response depends on the ratio of prey to predator, usually represented as $p(\frac{x}{y})$, which is supported by many field and laboratory observations, and is extensively applied in studying predator–prey models [Arditi & Ginzburg, 1989]. The qualitative investigation of ratio-dependent predator–prey models has shown that these models provide much richer and more reasonable dynamics than their traditional counterparts, and do not exhibit the paradox of enrichment [Kuang & Beretta, 1998; Kuang, 1999; Xiao & Ruan, 2001; Hsu *et al.*, 2001; Li & Kuang, 2007].

In the past studies, $q(\cdot)$ mainly takes three typical forms: (A) $q(x)=p(x)$ used in most predator–prey models [Holling, 1965], (B) $q(\frac{x}{y})=p(\frac{x}{y})$ used to represent more models in their performance to fit observed data [Abrams & Ginzburg, 2000], and (C) $q(\frac{y}{x})=s(1-\frac{u}{hx})$ used to analyze the general effect of harvesting [Xiao *et al.*, 2006]. Combining these different types of p and q functions yield many different predator–prey models to describe different situations. Nine predator–prey models with different response functions have been studied in [Jiang & Yu, 2017; Zeng *et al.*, 2020; Jiang *et al.*, 2020], described as

$$\mathrm{A_i}:\begin{cases}\dot{x}=rx\left(1-\dfrac{x}{K}\right)-mxy,\\[2mm] \dot{y}=y(mcx-d);\end{cases}$$

$$\mathrm{A_{ii}}:\begin{cases}\dot{x}=rx\left(1-\dfrac{x}{K}\right)-\dfrac{mxy}{a+x},\\[2mm] \dot{y}=y\left(\dfrac{mcx}{a+x}-d\right);\end{cases}$$

$$\mathrm{A_{iii}}:\begin{cases}\dot{x}=rx\left(1-\dfrac{x}{K}\right)-\dfrac{mx^2y}{ax^2+bx+1},\\[2mm] \dot{y}=y\left(\dfrac{mcx^2}{ax^2+bx+1}-d\right);\end{cases}$$

$$\mathrm{B_i}:\begin{cases}\dot{x}=rx\left(1-\dfrac{x}{K}\right)-mx,\\[2mm] \dot{y}=mcx-dy;\end{cases}$$

$$\mathrm{B_{ii}}:\begin{cases}\dot{x}=rx\left(1-\dfrac{x}{K}\right)-\dfrac{mxy}{x+ay},\\[2mm] \dot{y}=y\left(\dfrac{mcx}{x+ay}-d\right);\end{cases}$$

$$\mathrm{B_{iii}}:\begin{cases}\dot{x}=rx\left(1-\dfrac{x}{K}\right)-\dfrac{mx^2y}{ax^2+bxy+y^2},\\[2mm] \dot{y}=y\left(\dfrac{mcx^2}{ax^2+bxy+y^2}-d\right);\end{cases}$$

$$\mathrm{C_i}:\begin{cases}\dot{x}=rx\left(1-\dfrac{x}{K}\right)-mxy,\\[2mm] \dot{y}=sy\left(1-\dfrac{y}{hx}\right);\end{cases}$$

$$\mathrm{C_{ii}}:\begin{cases}\dot{x}=rx\left(1-\dfrac{x}{K}\right)-\dfrac{mxy}{a+x},\\[2mm] \dot{y}=sy\left(1-\dfrac{y}{hx}\right);\end{cases}$$

$$\mathrm{C_{iii}}:\begin{cases}\dot{x}=rx\left(1-\dfrac{x}{K}\right)-\dfrac{mx^2y}{ax^2+bx+1},\\[2mm] \dot{y}=sy\left(1-\dfrac{y}{hx}\right),\end{cases}$$

where different types of the functional response of the predator to the prey, including the Lotka–Volterra type, Holling type II and generalized Holling type III are used, while the function describing how the predator converts the consumed prey into the growth of predator is taken either as the same function of the predator to the prey, or that depending upon the ratio of the prey to the predator, or the ratio of predator to the prey. All parameters take positive real values, except $b > -2\sqrt{a}$. Dynamical properties including positivity of solutions, stability and bifurcation of equilibria and Hopf bifurcation are given in [Jiang & Yu, 2017] for models $\mathrm{A_i}$ through $\mathrm{B_{ii}}$, and in [Jiang *et al.*, 2020] for model $\mathrm{B_{iii}}$. Bogdanov–Takens bifurcation for models $\mathrm{A_{iii}}$ and $\mathrm{B_{iii}}$ are studied in [Zeng *et al.*, 2020].

The development of the traditional predator–prey models is based on the concept that when a population is at a low density, the fitness of an individual of species is high due to greater availability of resources; but as the population increases, the competition between individuals for resources increases and individual fitness declines. Thus, in the study of most classical predator–prey models, the effect of cooperation is neglected and it is assumed that the growth of prey population reaches its maximum at low densities and declines as population increases. However, the phenomenon called the Allee effect was discovered [Allee, 1932] because there exist many cooperative biological species that suffer a reduction in fitness at low population size due to lack of conspecifics. It was observed that species crashes to extinction if its population experiences a negative growth below a certain threshold level when the Allee effect is strong enough. The studies of the Allee effect have shown that it induces complex dynamics in predator–prey systems, for example, see [Verma & Misra, 2018]; and references therein. It was shown in these studies that inclusion of the Allee effect in ratio-dependent predator–prey models may reduce possible sustained oscillations of species and yield richer complex dynamical behaviors, causing an increase for the basin of attraction of extinction state and thus increasing the possibility of extinction of species.

An interesting phenomenon called prey refuge may decrease the risk of extinction of species by decreasing the predation risk. Many investigations have paid attention to the effect of prey refuge on the dynamics of predator–prey models without the Allee effect. It has been shown in most of these studies that prey refuge increases the equilibrium density of the prey and has a stabilizing effect on the predator–prey interaction. However, under a restricted set of conditions, refuge may have a destabilizing effect on the system dynamics [Ma *et al.*, 2009; Verma & Misra, 2018]. It is also found that the refuge which protects a constant number of prey has more stabilizing effect than the refuge which protects a constant proportion of prey. In [Rana *et al.*, 2014] the authors studied the impact of hiding behavior of prey and the Allee effect on discrete-time predator–prey models, showing that the Allee effect has a stabilizing effect on the system's dynamics for a moderate value of prey refuge. Recently, the combined effect of prey refuge with the Allee effect has been extensively studied by Verma and Misra [2018]. It is found that if prey refuge is less than the Allee threshold, the incorporation of prey refuge increases the threshold values of the predation rate and conversion efficiency at which unconditional extinction occurs. In addition, it is shown that if the prey refuge is greater than the Allee threshold, unconditional extinction may not be possible. Moreover, the study reveals that at a critical value of prey refuge, which is greater than the Allee threshold but less than the carrying capacity of prey population, the system undergoes a cusp bifurcation and exhibits complex dynamical behaviors.

In this paper, we will investigate the dynamics of four models among the above nine models with the Allee effect added. We want to compare the dynamical properties between the new models with the Allee effect and the models without the Allee effect. In particular, we will show new dynamical behavior due to the Allee effect. It will be noted that the dynamical analysis becomes much involved even for general stability and bifurcation analysis on equilibria. With the Allee effect added, the logistic growth function becomes

$$rx\left(1 - \frac{x}{K}\right)(x - e). \tag{2}$$

We assume that the Allee threshold is far from the carrying capacity so that the parameter e is assumed to lie in the interval $(0, \frac{K}{2})$ [Verma & Misra, 2018]. Then, applying a dimensionless process to the resulting equations, with $\tau = rKt$, $x = KX$, $D = \frac{d}{rK}$, $E = \frac{e}{K}$ and $S = \frac{s}{rK}$ (for simplicity, we still use dot to indicate the differentiation with the new time τ), we obtain the following nine dimensionless models:

$$\text{System A}_{\text{i}}: \begin{cases} \dot{X} = X(1-X)(X-E) - XY, \\ \dot{Y} = Y(CX - D), \end{cases} \quad Y = \frac{my}{rK}, \quad C = \frac{mc}{r};$$

$$\text{System A}_{\text{ii}}: \begin{cases} \dot{X} = X(1-X)(X-E) - \dfrac{XY}{A+X}, \\ \dot{Y} = Y\left(\dfrac{CX}{A+X} - D\right), \end{cases} \quad Y = \frac{my}{rK^2}, \quad A = \frac{a}{K}, \quad C = \frac{mc}{rK};$$

$$\text{System A}_{\text{iii}}: \begin{cases} \dot{X} = X(1-X)(X-E) - \dfrac{X^2Y}{AX^2+BX+1}, & Y = \dfrac{my}{r}, \quad A = K^2a, \\ \dot{Y} = Y\left(\dfrac{CX^2}{AX^2+BX+1} - D\right), & B = Kb, \quad C = \dfrac{mKc}{r}; \end{cases}$$

$$\text{System B}_{\text{i}}: \begin{cases} \dot{X} = X(1-X)(X-E) - MX, \\ \dot{Y} = X - DY, \end{cases} \quad Y = \frac{ry}{mc}, \quad M = \frac{m}{rK};$$

$$\text{System B}_{\text{ii}}: \begin{cases} \dot{X} = X(1-X)(X-E) - \dfrac{MXY}{X+Y}, \\ \dot{Y} = Y\left(\dfrac{CX}{X+Y} - D\right), \end{cases} \quad Y = \frac{ay}{K}, \quad M = \frac{m}{arK}, \quad C = \frac{mc}{rK};$$

$$\text{System B}_{\text{iii}}: \begin{cases} \dot{X} = X(1-X)(X-E) - \dfrac{MX^2Y}{X^2+BXY+Y^2}, & Y = \dfrac{y}{K\sqrt{a}}, \quad M = \dfrac{m}{rK\sqrt{a}}, \\ \dot{Y} = Y\left(\dfrac{CX^2}{X^2+BXY+Y^2} - D\right), & B = \dfrac{b}{\sqrt{a}}, \quad C = \dfrac{mc}{rKa}; \end{cases}$$

$$\text{System C}_{\text{i}}: \begin{cases} \dot{X} = X(1-X)(X-E) - MXY, \\ \dot{Y} = SY\left(1 - \dfrac{Y}{X}\right), \end{cases} \quad Y = \frac{y}{hK}, \quad M = \frac{hm}{r};$$

$$\text{System C}_{\text{ii}}: \begin{cases} \dot{X} = X(1-X)(X-E) - \dfrac{MXY}{A+X}, \\ \dot{Y} = SY\left(1 - \dfrac{Y}{X}\right), \end{cases} \quad Y = \frac{y}{hK}, \quad A = \frac{a}{K}, \quad M = \frac{hm}{rK};$$

$$\text{System C}_{\text{iii}}: \begin{cases} \dot{X} = X(1-X)(X-E) - \dfrac{MX^2Y}{AX^2+BX+1}, & Y = \dfrac{y}{hK}, \quad A = K^2a, \\ \dot{Y} = SY\left(1 - \dfrac{Y}{X}\right), & B = Kb, \quad M = \dfrac{hKm}{r}, \end{cases}$$

where $0 < E < \frac{1}{2}$, and $\frac{B}{\sqrt{A}} > -2$ for systems A_{iii} and C_{iii}, while $B > -2$ for system B_{iii}.

In this paper, we will consider the four models A_i, A_{ii}, B_i and B_{ii}. It was shown in [Jiang & Yu, 2017] that without the Allee effect, all the four models have no B–T bifurcation, and only models A_{ii} and B_{ii} have codimension-one Hopf bifurcation. In this paper, besides bifurcation and stability analysis, we will show that with the Allee effect, the model A_i also has codimension-one Hopf bifurcation, and the models A_i, A_{ii} and B_i still do not have B–T bifurcation, but the model B_{ii} has codimension-two B–T bifurcation. Moreover, it is shown that with the Allee effect, the trivial equilibrium solution — the origin $(0, 0)$ in the model B_{ii} becomes a stable node for all parameter values, while that in the model B_{ii} without the Allee effect has very complex dynamics around it [Xiao & Ruan, 2001]. Also, it is interesting to note that for the model B_{ii}, the supercritical Hopf bifurcation generated under no Allee effect is changed to a subcritical Hopf bifurcation under the Allee effect, and thus the stable limit cycle becomes unstable, leading to the stable domain of the trajectories being increased.

Before giving detailed discussions on the four models one by one, we prove the positivity of the solutions of the models. Moreover, we also show that these solutions are bounded.

Theorem 1.1. *The solutions of the systems* A_i, A_{ii} B_i *and* B_{ii} *are positive provided the initial conditions are positive. Moreover, these solutions are bounded and eventually attracted to a trapping region.*

Proof. Since the proofs for the four models are similar, we do not repeat all of them, but only show the proof for model A_i.

Using the method of constant variations, we can write the general solution of system A_i with the initial values $X(0)$ and $Y(0)$ as

$$\begin{aligned} X(\tau) &= X(0)\exp\left\{\int_0^\tau [(1-X(s)) \right. \\ &\qquad \left. \times (X(s)-E) - Y(s)]ds\right\}, \qquad (3) \\ Y(\tau) &= Y(0)\exp\left\{\int_0^\tau [CX(s)-D]ds\right\}, \end{aligned}$$

which clearly indicates that $X(\tau) > 0$, $Y(\tau) > 0$ for any $\tau > 0$, if $X(0) > 0$ and $Y(0) > 0$.

Next, we prove that these solutions are bounded and eventually attracted to a right triangle trapping region Ω_{A_i}, defined by

$$\begin{aligned} \Omega_{A_i} = \left\{ (X,Y) | X > 0, Y > 0, \right. \\ \left. Y < C\max\left\{\frac{1-E}{D}, 1\right\} - CX \right\}, \end{aligned} \qquad (4)$$

which is bounded by the X-axis, the Y-axis and the straight line: $Y + CX = C\max\{\frac{1-E}{D}, 1\}$. Now, consider the line L, defined by

$$\mathrm{L}:\ Y + CX = \overline{C} \geq C\max\left\{\frac{1-E}{D}, 1\right\}, \qquad (5)$$

which implies that the line L is above the trapping region Ω_{A_i}.

To prove that all trajectories are attracted into the trapping region Ω_{A_i}, we construct the function,

$$F = \frac{1}{D}(Y + CX). \qquad (6)$$

Since both X-axis and Y-axis are invariant, we only need to prove that $\frac{dF}{d\tau} < 0$ along the trajectories on the line L. Simple calculation shows that the *transversality condition* is given by

$$\begin{aligned} \frac{dF}{d\tau} &= \frac{1}{D}(C\dot{X} + \dot{Y}) \\ &= \frac{C}{D}X(1-X)(X-E) - Y. \end{aligned} \qquad (7)$$

Consider the planar curve on the X–Y plane, defined by the equation:

$$\mathrm{S}:\ \frac{C}{D}X(1-X)(X-E) - Y = 0, \qquad (8)$$

which passes through the X-axis at the points: $(0, 0)$, $(E, 0)$ and $(1, 0)$, as shown in Fig. 1, where the red curve is S, the green line is L, and the blue curve denotes the tangent line T to S, passing through the point $(1, 0)$ on S.

It is easy to see that $\frac{dF}{d\tau} > 0$ (< 0) in the region below (above) the curve S, and it can be shown that the slope of the tangent line T at the point $(1, 0)$ is $-\frac{C(1-E)}{D}$. Thus, $\frac{dF}{d\tau} < 0$ on the line L. In fact, it is easy to see from (7) that $\frac{dF}{d\tau} < 0$ for $0 < X < E$ and $X > 1$, and the line $X = 1$ can serve as a part of the boundary of Ω_{A_i} [see Fig. 1(b)]. But for $E < X < 1$, in the region bounded by the curve S and the X-axis, $\frac{dF}{d\tau} > 0$. That is why the line L must enclose the curve S. More precisely, we may find the line L which is just tangent to the curve S, but its expression is more involved.

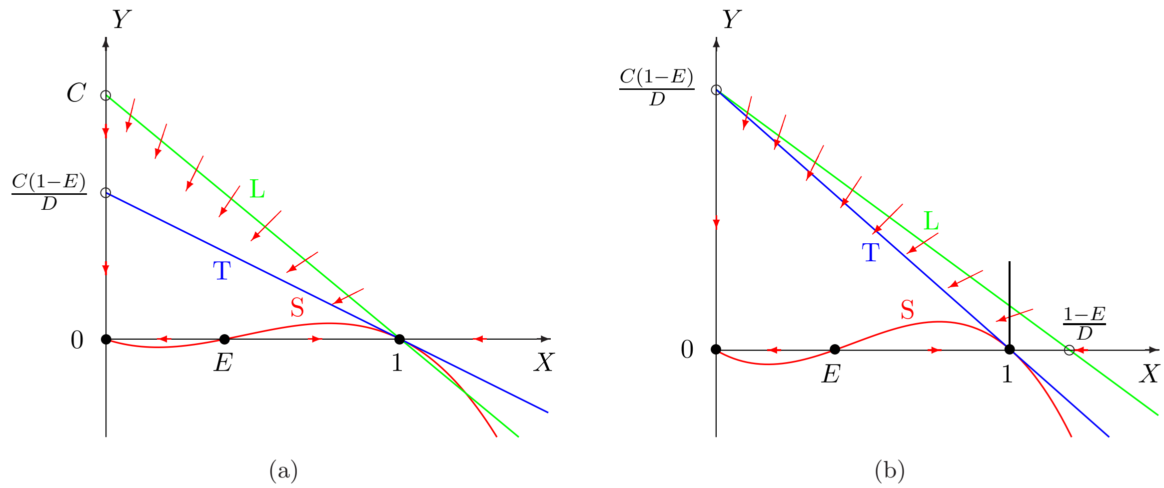

Fig. 1. Graph of the line L with $\overline{C} = C\max\{\frac{1-E}{D}, 1\}$, the curve S and the tangent line T to S, passing through the point $(1, 0)$ for (a) $D > 1 - E$ and (b) $D \le 1 - E$.

The trapping region Ω_{A_1} can also be used for proving the boundedness of system A_{ii}. To prove the boundedness of system B_i, one can modify the line L as $Y + \frac{1}{M}X = \frac{1}{M}\max\{\frac{1-E}{D}, 1\}$; and similarly the line L can be changed to $Y + \frac{C}{M}X = \frac{C}{M}\max\{\frac{1-E}{D}, 1\}$ for proving the boundedness of system B_{ii}. ■

The rest of the paper is organized as follows. In the next four sections, we will respectively study the models A_i, A_{ii}, B_i and B_{ii} on the property of solutions, equilibrium solutions and their stability, and bifurcations from the equilibrium solutions. At the beginning of each section, we will summarize the results of the model without the Allee effect, taken from [Jiang & Yu, 2017], in order to give a comparison with those results obtained for the model with the Allee effect. Simulations are presented in Sec. 5, and finally conclusion is drawn in Sec. 6.

2. Dynamics and Bifurcations of System A_i

Now we consider the system A_i. First, we list the existing results for the system without the Allee effect in order to give a comparison.

2.1. *The results for system A_i without the Allee effect*

The system without the Allee effect is described by

$$\begin{aligned} \dot{X} &= X(1 - X) - XY, \\ \dot{Y} &= Y(CX - D), \end{aligned} \tag{9}$$

which has three equilibrium solutions. The solutions and their stability [Jiang & Yu, 2017] are given below:

$$\begin{aligned} &E_0 = (0, 0), \quad \text{Saddle}, \\ &E_1 = (1, 0), \quad \text{GAS for } \frac{D}{C} \ge 1, \\ &E_3 = \left(\frac{D}{C}, 1 - \frac{D}{C}\right), \quad \text{GAS for } 0 < \frac{D}{C} < 1, \end{aligned} \tag{10}$$

where GAS stands for Globally Asymptotically Stable. The notation on the numbers of equilibria follows that for the system with the Allee effect in order to have an easy comparison. It is clear that the system A_i without the Allee effect does not have complex dynamical behaviors, which has either a GAS equilibrium E_1 or a GAS equilibrium E_3, depending upon the ratio $\frac{D}{C}$. The bifurcation diagram is shown in Fig. 2(a), which is placed together with the bifurcation diagram for system A_i with the Allee effect for a convenient comparison.

2.2. *Stability and bifurcations of equilibria of system A_i with the Allee effect*

Now we turn to system A_i with the Allee effect, which is given by

$$A_i: \begin{cases} \dot{X} = X(1 - X)(X - E) - XY, \\ \dot{Y} = Y(CX - D). \end{cases} \tag{11}$$

The equilibrium solutions of this system can be easily obtained by setting $\dot{X} = \dot{Y} = 0$, as given by

$$\begin{aligned}
&\mathrm{E}_0: \ (X_0, Y_0) = (0, 0),\\
&\mathrm{E}_1: \ (X_1, Y_1) = (1, 0),\\
&\mathrm{E}_2: \ (X_2, Y_2) = (E, 0),\\
&\mathrm{E}_3: \ (X_3, Y_3) = \left(\frac{D}{C}, \left(1 - \frac{D}{C}\right)\left(\frac{D}{C} - E\right)\right).
\end{aligned} \tag{12}$$

The equilibrium solutions E_0, E_1 and E_2 exist for positive parameter values, while E_3 exists for $E < \frac{D}{C} < 1$. It is seen that system $\mathrm{A_i}$ with the Allee effect has one more equilibrium E_2 than that of the system without the Allee effect.

For $\mathrm{A_i}$ system with the Allee effect, we have the following theorem for the stability and bifurcations of these equilibrium solutions.

Theorem 2.1. *For system* $\mathrm{A_i}$, E_0 *is a stable node and globally asymptotically stable for* $\frac{D}{C} < E$; E_1 *is a stable node when* $\frac{D}{C} > 1$ *and a saddle point when* $\frac{D}{C} < 1$; E_2 *is a saddle point when* $\frac{D}{C} > E$, *and an unstable node when* $\frac{D}{C} < E$. E_3 *exists for* $E < \frac{D}{C} < 1$, *and it is a stable focus for* $\frac{1+E}{2} < \frac{D}{C} < 1$ *and an unstable focus for* $E < \frac{D}{C} < \frac{1+E}{2}$; *Hopf bifurcation occurs from* E_3 *at the critical point* $[\frac{D}{C}]_{\mathrm{H}} = \frac{1+E}{2}$. *The system has no B–T bifurcation.*

Proof. The stability of these equilibrium solutions is determined from the Jacobian matrix of the system, given by

$$J(X, Y) = \begin{bmatrix} -E - 3X^2 + 2(1+E)X - Y & -X \\ CY & CX - D \end{bmatrix}. \tag{13}$$

Evaluating the Jacobian J on the equilibrium E_0 yields two eigenvalues: $-E < 0$ and $-D < 0$, indicating that E_0 is a stable node. In fact, the corresponding two eigenvectors are along the X-axis and the Y-axis since the X- and Y-axes are invariant.

Similarly, evaluating the Jacobian J on E_1, we obtain two eigenvalues: $-(1-E) < 0$ and $C - D$. So E_1 is a stable node when $\frac{D}{C} > 1$ and a saddle point when $\frac{D}{C} < 1$. Next, evaluating the Jacobian J on E_2, we obtain two eigenvalues: $E(1-E) > 0$ and $CE - D$. So E_2 is a saddle point when $\frac{D}{C} > E$ and an unstable node when $\frac{D}{C} < E$.

For the equilibrium E_3 which exists for $E < \frac{D}{C} < 1$, we have the Jacobian matrix:

$$J_3 = \begin{bmatrix} \dfrac{D}{C}\left(1 + E - \dfrac{2D}{C}\right) & -\dfrac{D}{C} \\ C\left(1 - \dfrac{D}{C}\right)\left(\dfrac{D}{C} - E\right) & 0 \end{bmatrix}$$

which yields the determinant and trace as

$$\det(J_3) = D\left(1 - \frac{D}{C}\right)\left(\frac{D}{C} - E\right) > 0, \quad \text{when } E_3 \text{ exists}, \tag{14}$$

$$\mathrm{Tr}(J_3) = \frac{D}{C}\left(1 + E - \frac{2D}{C}\right).$$

Hence, E_3 is stable (unstable) if $\mathrm{Tr}(J_3) < 0$ (> 0), i.e. if $\frac{1+E}{2} < \frac{D}{C} < 1$ ($E < \frac{D}{C} < \frac{1+E}{2}$). Since $\det(J_3) > 0$, B–T bifurcation is not possible.

At the critical point, $[\frac{D}{C}]_{\mathrm{H}} = \frac{1+E}{2}$, J_3 has a purely imaginary pair. Moreover, a simple calculation shows that the transversality condition is given by

$$\mathrm{T_{trans}} = \frac{1}{2}\frac{d\,\mathrm{Tr}(J_3)}{d\left(\dfrac{D}{C}\right)}\Bigg|_{[\frac{D}{C}]_{\mathrm{H}}} = -\frac{1+E}{2} < 0, \tag{15}$$

implying that Hopf bifurcation occurs from E_3 at the critical point $\frac{D}{C} = [\frac{D}{C}]_{\mathrm{H}}$.

To prove that the equilibrium E_0 is globally asymptotically stable for $\frac{D}{C} < E$, note that the equilibria E_0, E_1 and E_2 are all boundary equilibria, while E_3 is an interior point if it exists. Since for $\frac{D}{C} < E$, E_3 does not exist, and E_1 and E_2 are unstable, so the only stable equilibrium is E_0 on the boundary of the trapping region. Thus, all trajectories would converge to E_0. ■

2.3. *Codimension of Hopf bifurcation*

Next, we prove that the Hopf bifurcation is supercritical and bifurcating limit cycles are stable. Moreover, we show that the codimension of the Hopf bifurcation is one. We have the following theorem.

Theorem 2.2. *For the system* $\mathrm{A_i}$, *Hopf bifurcation occurs from* E_3 *at the critical point* $[\frac{D}{C}]_{\mathrm{H}} = \frac{1+E}{2}$, *and it is supercritical with stable bifurcating limit cycles. Moreover, the codimension of Hopf bifurcation is one.*

Proof. We apply normal form theory to find the focus value. To achieve this, without of loss of generality, we may use the critical value $\frac{D}{C} = [\frac{D}{C}]_{\rm H}$ to let $D = \frac{C(1+E)}{2}$, and then introduce the affine transformation:

$$X = \frac{1+E}{2} + x_1, \quad Y = \frac{1}{4}(1-E)^2 - \frac{2\omega_c}{1+E}x_2,$$

where $\omega_c = \frac{1}{2\sqrt{2}}(1-E)\sqrt{C(1+E)}$, into system (11) to obtain

$$\begin{aligned}\dot{x}_1 &= \omega_c x_2 - \frac{1+E}{2}x_1^2 + \frac{2\omega_c}{1+E}x_1x_2 - x_1^3 \\ &\triangleq f(x_1, x_2), \\ \dot{x}_2 &= -\omega_c x_1 + Cx_1x_2 \triangleq g(x_1, x_2).\end{aligned}$$

Then, we may either apply the Maple program in [Yu, 1998] or directly use the following formula to get the first-order focus value, evaluated at $(x_1, x_2) = (0, 0)$:

$$\begin{aligned}v_1 &= \frac{1}{16}\left(\frac{\partial^3 f}{\partial x_1^3} + \frac{\partial^3 f}{\partial x_1 \partial x_2^2} + \frac{\partial^3 g}{\partial x_1^2 \partial x_2}\frac{\partial^3 g}{\partial x_2^3}\right) \\ &\quad - \frac{1}{16\omega_c}\left[\frac{\partial^2 f}{\partial x_1 \partial x_2}\left(\frac{\partial^2 f}{\partial x_1^2} + \frac{\partial^2 f}{\partial x_2^2}\right)\right. \\ &\quad - \frac{\partial^2 g}{\partial x_1 \partial x_2}\left(\frac{\partial^2 g}{\partial x_1^2} + \frac{\partial^2 g}{\partial x_2^2}\right) \\ &\quad \left. - \frac{\partial^2 f}{\partial x_1^2}\frac{\partial^2 g}{\partial x_1^2} + \frac{\partial^2 f}{\partial x_2^2}\frac{\partial^2 g}{\partial x_2^2}\right] \\ &= -\frac{6}{16} + \frac{1}{16\omega_c}\left[\frac{2\omega_c}{1+E}(1+E)\right] \\ &= -\frac{1}{4},\end{aligned} \tag{16}$$

which holds negative for any positive parameter values, indicating that the codimension of Hopf bifurcation is one, and it is supercritical with stable bifurcating limit cycles for $\frac{D}{C} \in (E, \frac{1+E}{2})$. ■

2.4. *Bifurcation diagram and simulation*

Based on Theorem 2.1, we choose X as the state variable and $\frac{D}{C}$ as the bifurcation parameter to obtain the bifurcation diagram, as shown in Fig. 2(b). It can be seen from this figure that there exist bistable states $(\mathrm{E}_0, \mathrm{E}_1)$ for $\frac{D}{C} > 1$, and states $(\mathrm{E}_0, \mathrm{E}_3)$ for $\frac{1+E}{2} < \frac{D}{C} < 1$. There is a transcritical bifurcation between E_0 and E_1 at $\frac{D}{C} = 1$, and a Hopf bifurcation from E_3 at $\frac{D}{C} = \frac{1+E}{2}$. T and H denote the transcritical bifurcation and Hopf bifurcation, respectively.

Now we present simulations for the model $\mathrm{A_i}$. Since the bifurcation diagrams in Fig. 2 have shown the difference between the models without the Allee effect and with the Allee effect, we shall only present the results for the model with the Allee effect, which display more complex dynamical behaviors. We take the following parameter values for simulation:

$$E = 0.4, \quad \frac{D}{C} = 0.2, 0.68, 0.8, 1.2.$$

In simulation we take $C = 1$ for simplicity. The Hopf critical point is at $\frac{1+E}{2} = 0.7$. Hence, the equilibrium E_3 only exists for $\frac{D}{C} \in (0.4, 1)$ and it is stable for $0.7 < \frac{D}{C} < 1$ and unstable for $0.4 < \frac{D}{C} < 0.7$. Therefore, the bistable phenomenon exists for $\frac{D}{C} > 0.7$, for which two stable equilibria E_0 and E_3 coexist for $0.7 < \frac{D}{C} < 1$, and two stable equilibria E_0 and E_1 coexist for $\frac{D}{C} > 1$. Moreover, since the Hopf bifurcation is supercritical, yielding stable limit cycles, another bistable phenomenon involving the stable equilibrium E_0 and a stable limit cycle near the Hopf critical point for $\frac{D}{C} < \frac{1+E}{2}$ can also occur. Note that the unstable equilibrium $\mathrm{E}_2 : (0.4, 0)$ is between the two stable equilibria E_0 and E_1. So at the bistable situations, choosing different initial points may converge to different equilibria. The simulations are given in Fig. 3, indicating an excellent agreement with the analytical predictions which are shown in the bifurcation diagram [see Fig. 2(b)].

Remark 2.3. Comparing bifurcation diagram in Fig. 2(b) (with the Allee effect) with that in Fig. 2(a) (without the Allee effect) we can see that the Allee effect has a great impact on the dynamical behaviors of the system. First of all, note that the model without the Allee effect does not exhibit complex behaviors, it either has a globally asymptotically stable equilibrium E_1 if $\frac{D}{C} > 1$ or a globally asymptotically stable equilibrium E_3 if $\frac{D}{C} < 1$. Only a transcritical bifurcation occurs between E_1 and E_3 at $\frac{D}{C} = 1$, see Fig. 2(a). However, for the model with the Allee effect, except for no change

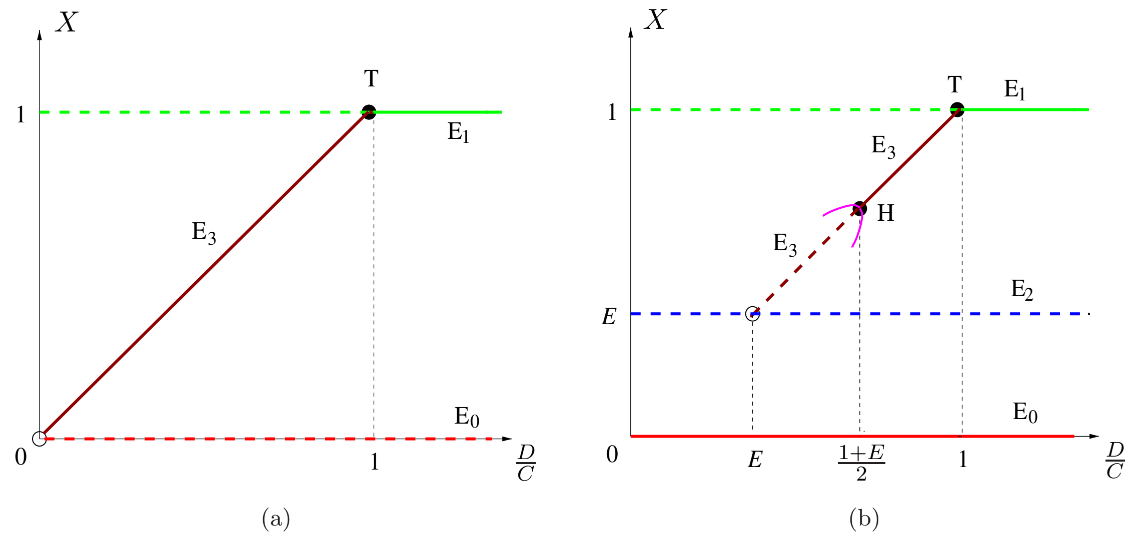

Fig. 2. Bifurcation diagrams for system $\mathrm{A_i}$: (a) without the Allee effect and (b) with the Allee effect, where the solid pink curve denotes the supercritical Hopf bifurcation.

on the equilibrium $\mathrm{E_1}$, we have the following interesting observations.

(1) A new unstable equilibrium $\mathrm{E_2} = (E, 0)$ emerges due to the Allee effect, which causes the stability change of the equilibrium $\mathrm{E_0}$ from unstable to stable. In other words, due to the Allee effect, solutions near $\mathrm{E_0}$ now converge to $\mathrm{E_0}$, implying that a strong Allee effect can cause species to extinct, in particular when $\frac{D}{C} < E$, as shown in Figs. 2 and 3.

(2) The positive (interior) equilibrium $\mathrm{E_3}$ now exists only for $E < \frac{D}{C} < 1$, while $\mathrm{E_0}$ is globally asymptotically stable for $0 < \frac{D}{C} < E$. Moreover, $\mathrm{E_3}$ is only stable for $\frac{1+E}{2} < \frac{D}{C} < 1$. This implies that the Allee effect destabilizes the positive equilibrium for intermediate values of $\frac{D}{C}$, see Figs. 2 and 3(b).

(3) Complex dynamics including bistable phenomena occurs. One kind of the bistable phenomena includes two stable equilibria: $\mathrm{E_0}$ and $\mathrm{E_3}$ for slightly larger $\frac{D}{C} \in (\frac{1+E}{2}, 1)$, and $\mathrm{E_0}$ and $\mathrm{E_1}$ for $\frac{D}{C} > 1$. Solutions converge to either $\mathrm{E_0}$ or $\mathrm{E_3}$ for the former, and $\mathrm{E_0}$ or $\mathrm{E_1}$ for the latter, depending upon the initial conditions. These two bistable phenomena are shown in Figs. 2, 3(c) and 3(d). The other kind of bistable phenomenon, due to Hopf bifurcation, involves the stable equilibrium $\mathrm{E_0}$ and a stable limit cycle for slightly larger $\frac{D}{C} \in (E, \frac{1+E}{2})$, and solutions converge to either the equilibrium $\mathrm{E_0}$ or the stable limit cycle, depending on the initial condition, see Figs. 2 and 3(b).

(4) Note that the Hopf critical point is always the midpoint of the interval $\frac{D}{C} \in (E, 1)$ for which $\mathrm{E_3}$ exists. As $E \to 0$, the Hopf bifurcation exists as long as $E > 0$. It shows a discontinuity (jumping) from the case $E = 0$ to the case $E > 0$, because when $E = 0$, the model does not have the term $(X - E)$ on the first equation. Thus, as $E \to 0$, the unstable $\mathrm{E_2}$ coincides with $\mathrm{E_0}$ which then becomes unstable; while as E goes to its maximal value $\frac{1}{2}$, $\mathrm{E_0}$ becomes more stable, and the Hopf critical point on $\mathrm{E_3}$ moves towards $[\frac{D}{C}]_{\mathrm{H}} = \frac{3}{4}$, and it becomes less stable.

3. Dynamics and Bifurcations of System $\mathrm{A_{ii}}$

In this section, we consider the model $\mathrm{A_{ii}}$. Similarly, we first summarize the existing results on this system without the Allee effect.

3.1. *The results for the system* $\mathrm{A_{ii}}$ *without the Allee effect*

The model $\mathrm{A_{ii}}$ without the Allee effect is described by

$$\begin{aligned} \dot{X} &= X(1 - X) - \frac{XY}{A + X}, \\ \dot{Y} &= Y\left(\frac{CX}{A + X} - D\right), \end{aligned} \tag{17}$$

which has three equilibrium solutions. The solutions and their stability [Jiang & Yu, 2017] are given

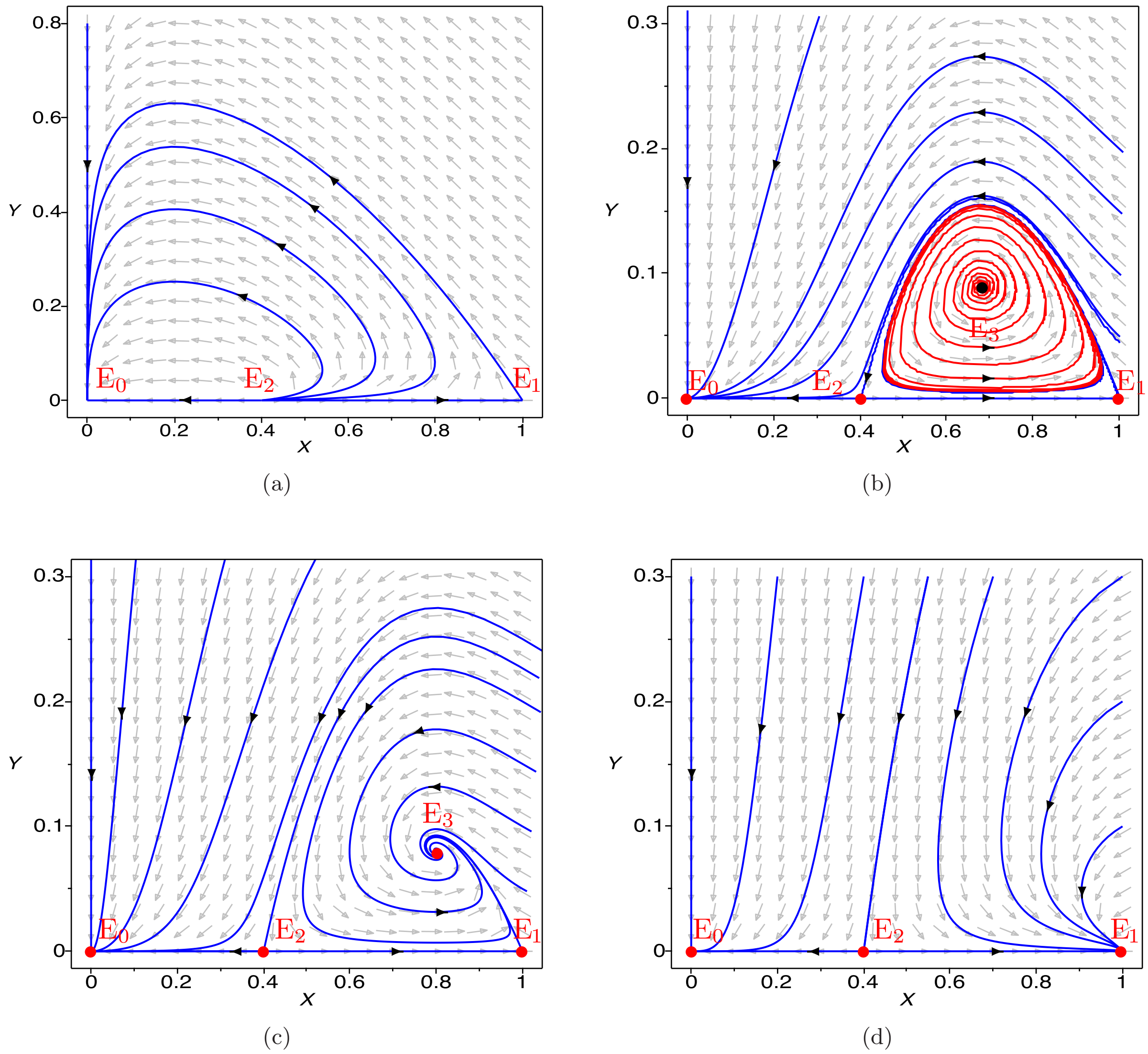

Fig. 3. Simulated phase portraits for the model A_i with $E = 0.4$, $C = 1$: (a) $D = 0.2$, converging to E_0, (b) $D = 0.68$, converging to E_0 or a stable limit cycle, (c) $D = 0.8$, converging to E_0 or E_3 and (d) $D = 1.2$, converging to E_0 or E_1.

below:

$$
\begin{aligned}
&E_0 = (0,0), \quad \text{Saddle},\\
&E_1 = (1,0), \quad \text{GAS for } A \geq \max\left\{0, \frac{C}{D} - 1\right\},\\
&E_3 = \left(\frac{AD}{C-D}, \frac{AC[C-(A+1)D]}{(C-D)^2}\right),\\
&\qquad\qquad \text{GAS for } 0 < A < \frac{C}{D} - 1.
\end{aligned} \tag{18}
$$

It is seen that like system A_i without the Allee effect, system A_{ii} without the Allee effect does not have complex dynamical behaviors, which has either a GAS equilibrium E_1 or a GAS equilibrium E_3 depending on the value of $\frac{D}{C} - 1$. The bifurcation diagram is depicted in Fig. 4(a), where it is assumed $C > D$; otherwise, E_3 does not exist and E_1 is globally asymptotically stable.

3.2. *Stability and bifurcations of equilibria of system A_{ii} with the Allee effect*

The model A_{ii} with the Allee effect is given by

$$
A_{ii}: \begin{cases} \dot{X} = X(1-X)(X-E) - \dfrac{XY}{A+X}, \\[2mm] \dot{Y} = Y\left(\dfrac{CX}{A+X} - D\right), \end{cases} \tag{19}
$$

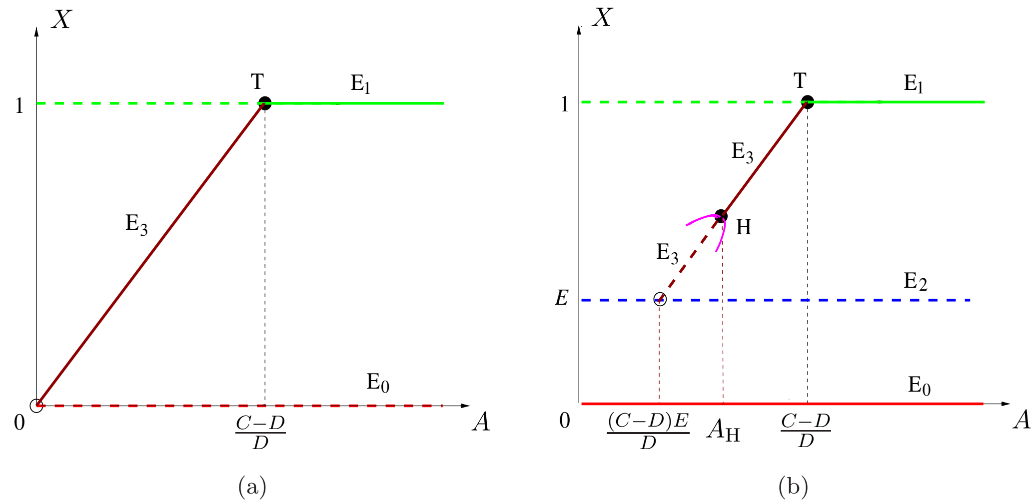

Fig. 4. Bifurcation diagrams for system $\mathrm{A_{ii}}$: (a) without the Allee effect and (b) with the Allee effect, where the solid pink curve denotes the supercritical Hopf bifurcation.

The equilibrium solutions of this system can be easily found by setting $\dot{X} = \dot{Y} = 0$ as

$$\begin{aligned} &\mathrm{E}_0 : (X_0, Y_0) = (0, 0), \\ &\mathrm{E}_1 : (X_1, Y_1) = (1, 0), \\ &\mathrm{E}_2 : (X_2, Y_2) = (E, 0), \\ &\mathrm{E}_3 : (X_3, Y_3), \quad \text{where } X_3 = \frac{AD}{C-D}, \\ &\qquad Y_3 = (1 - X_3)(X_3 - E)(A + X_3). \end{aligned} \tag{20}$$

The equilibrium solutions E_0, E_1 and E_2 exist for positive parameter values, while E_3 exists for

$$C > D, \quad \frac{(C-D)E}{D} < A < \frac{C-D}{D}, \tag{21}$$

since $E < X_3 < 1$ due to $Y_3 > 0$.

We have the following result.

Theorem 3.1. *For system* $\mathrm{A_{ii}}$, E_0 *is a stable node*; E_1 *is either a stable node if* $A > \max\{0, \frac{C}{D} - 1\}$ *or a saddle point if* $0 < A < \frac{C}{D} - 1$; E_2 *is unstable* (*either a saddle point or an unstable node*). E_3 *exists when the condition* (*21*) *is satisfied, and is asymptotically stable for* $A_{\mathrm{H}} < A < \frac{C-D}{D}$, *where*

$$A_{\mathrm{H}} = \frac{C-D}{2D(2C+D)}\big[(1+E)(C+D) + \sqrt{(1-E)^2(C+D)^2 + 4EC^2}\big]. \tag{22}$$

Hopf bifurcation occurs from E_3 *at the critical point* A_{H}. *There does not exist B–T bifurcation.*

Proof. Similarly, with the Jacobian of the system, given by

$$J(X,Y) = \begin{bmatrix} -E + 2(1+E)X - 3X^2 - \dfrac{AY}{(A+X)^2} & -\dfrac{X}{A+X} \\ \dfrac{ACY}{(A+X)^2} & \dfrac{CX}{A+X} - D \end{bmatrix},$$

we can determine the stability of these equilibrium solutions.

Evaluating the Jacobian J on the equilibrium E_0 we have two negative eigenvalues: $-E$ and $-D$, implying that E_0 is a stable node. Again note that the X- and Y-axes are invariant.

Similarly, evaluating the Jacobian J on E_1 yields two eigenvalues: $-(1-E) < 0$ and $\frac{C}{A+1} - D$. So E_1 is a stable node if $A > \max\{0, \frac{C}{D} - 1\}$ and a saddle point if $0 < A < \frac{C}{D} - 1$. Next, evaluating the Jacobian J on E_2, we obtain two eigenvalues: $E(1-E) > 0$ and $\frac{CE}{A+E} - D$. Thus, E_2 is a saddle point if $A > \max\{0, (\frac{C}{D} - 1)E\}$, and an unstable node if $0 < A < \frac{C}{D} - 1$.

For the equilibrium E_3 which exists for $0 < \frac{(C-D)E}{D} < A < \frac{C-D}{D}$, we evaluate the Jacobian J on E_3, which in turn yields the determinant and trace as follows:

$$\begin{aligned}\det(J_3) &= \frac{D^3}{C(C-D)}\left[A - \frac{(C-D)E}{D}\right]\\ &\quad\times\left(\frac{C-D}{D} - A\right),\\ \mathrm{Tr}(J_3) &= -\frac{D}{C(C-D)^2}\{D(2C+D)A^2\\ &\quad-(1+E)(C^2-D^2)A + E(C-D)^2\}.\end{aligned} \tag{23}$$

Obviously, $\det(J_3) > 0$ for existing E_3. Therefore, E_3 is asymptotically stable if $\mathrm{Tr}(J_3) < 0$. Let

$$\begin{aligned}F_{\mathrm{A_{ii}}} &= D(2C+D)A^2 - (1+E)(C^2-D^2)A\\ &\quad+E(C-D)^2,\end{aligned} \tag{24}$$

which is a quadratic polynomial in A with the discriminant,

$$\begin{aligned}\Delta_{\mathrm{A_{ii}}} &= (1+E)^2(C^2-D^2)^2\\ &\quad-4ED(2C+D)(C-D)^2\\ &= (C-D)^2[(1-E)^2(C+D)^2 + 4EC^2]\\ &> 0.\end{aligned}$$

Thus, $F = 0$ has two real positive roots:

$$\begin{aligned}A_\pm &= \frac{C-D}{2D(2C+D)}[(1+E)(C+D)\\ &\quad\pm\sqrt{(1-E)^2(C+D)^2+4EC^2}].\end{aligned} \tag{25}$$

Due to the existence condition (21), it requires that at least one of $A_\pm$ must belong to the interval $(\frac{(C-D)E}{D}, \frac{C-D}{D})$. A simple calculation shows that

$$\begin{aligned}A_\pm - \frac{(C-D)E}{D} &= \frac{C-D}{2D(2C+D)}[(C+D) - E(3C+D) \pm \sqrt{(1-E)^2(C+D)^2+4EC^2}]\\ &= \frac{4E(1-E)C(C-D)}{2D\{-[(C+D)-E(3C+D)] \pm \sqrt{(1-E)^2(C+D)^2+4EC^2}\}}.\end{aligned} \tag{26}$$

We first prove $A_- < \frac{(C-D)E}{D}$, and so $A_- \notin (\frac{(C-D)E}{D}, \frac{C-D}{D})$. Note that $\frac{C+D}{3C+D} < \frac{1}{2}$ for $C > D$. Thus, if $\frac{C+D}{3C+D} \le E$, we have $(C+D) - E(3C+D) < 0$ and so the first equation in (26) implies $A_- < \frac{(C-D)E}{D}$. If $E < \frac{C+D}{3C+D} < \frac{1}{2}$, we have $(C+D) - E(3C+D) > 0$, and then the second equation in (26) also implies $A_- < \frac{(C-D)E}{D}$.

Next, we prove $A_+ \in (\frac{(C-D)E}{D}, \frac{C-D}{D})$. To show $A_+ > \frac{(C-D)E}{D}$, we notice that $(C+D) - E(3C+D) > 0$ for $\frac{C+D}{3C+D} > E$, so the first equation in (26) implies $A_+ > \frac{(C-D)E}{D}$; while for $\frac{C+D}{3C+D} \le E < \frac{1}{2}$, we have $(C+D) - E(3C+D) \le 0$, so the second equation in (26) again leads to $A_+ > \frac{(C-D)E}{D}$. To prove $A_+ < \frac{C-D}{D}$, we can similarly obtain that

$$\begin{aligned}A_+ - \frac{C-D}{D} &= \frac{C-D}{2D(2C+D)}\{\sqrt{(1-E)^2(C+D)^2+4EC^2} - [(1-E)(C+D)+2C]\}\\ &= -\frac{4(1-E)C(C-D)}{2D[\sqrt{(1-E)^2(C+D)^2+4EC^2} + (1-E)(C+D)+2C]},\end{aligned} \tag{27}$$

which clearly indicates that $A_+ < \frac{C-D}{D}$. Hence, $A_+ \in (\frac{(C-D)E}{D}, \frac{C-D}{D})$ for $0 < E < \frac{1}{2}$.

Let $A_{\mathrm{H}} = A_+$. Then, concluding the above discussions we know that the equilibrium E_3 exists for $\frac{(C-D)E}{D} < A < \frac{C-D}{D}$, and it is asymptotically stable for $A_{\mathrm{H}} < A < \frac{C-D}{D}$, and unstable for $\frac{(C-D)E}{D} < A < A_{\mathrm{H}}$. Further, we can use (23) to find the transversality condition as follows:

$$\begin{aligned}\mathrm{T_{trans}} = \frac{1}{2}\frac{d\,\mathrm{Tr}(J_3)}{dA}\bigg|_{A=A_{\mathrm{H}}} &= -\frac{D}{2C(C-D)^2}[2D(2C+D)A_{\mathrm{H}} - (1+E)(C^2-D^2)]\\ &= -\frac{D}{2C(C-D)}\sqrt{(1-E)^2(C+D)^2+4EC^2} < 0,\end{aligned}$$

implying that Hopf bifurcation occurs from the equilibrium E_3 at the critical point $A = A_H$. Note that B–T bifurcation cannot happen since $\det(J_3) > 0$ when E_3 exists. ■

3.3. *Codimension of the Hopf bifurcation*

Now we further study the Hopf bifurcation and determine the codimension of the Hopf bifurcation. We have the following theorem.

Theorem 3.2. *For system* A_{ii}, *Hopf bifurcation occurs from* E_3 *at the critical point* $A = A_H$. *The Hopf bifurcation is supercritical and bifurcating limit cycles are stable. Moreover, the codimension of Hopf bifurcation is one.*

Proof. In order to determine the stability of bifurcating limit cycles, similar to the analysis for the system A_i, we apply the method of normal forms. To have an affine transformation for system (19) at the critical point $A = A_H$, since $F_{A_{ii}}$ in (24) is a quadratic polynomial in A, we use E, instead of A, to solve $F_{A_{ii}} = 0$ for the convenience in normal form computation. Thus, solving $F_{A_{ii}} = 0$ for E yields

$$E_H = \frac{A[D(2C+D)A - (C^2 - D^2)]}{(C-D)[(C+D)A - (C-D)]}.$$

In order to have $E_H \in (0, \frac{1}{2})$, the following conditions must hold:

$$E_H > 0 \Rightarrow A < \frac{C-D}{C+D}A_1 \quad \text{or}$$

$$A > \frac{C^2 - D^2}{D(2C+D)} \triangleq A_2$$

and

$$\begin{aligned} E_H < \frac{1}{2} &\Leftrightarrow 2D(2C+D)A^2 - 3(C^2 - D^2)A + (C-D)^2 < 0 \\ &\Leftrightarrow A_n \triangleq \frac{(C-D)[3(C+D) - \sqrt{8C^2 + (C+D)^2}]}{4D(2C+D)} < A \\ &\qquad < \frac{(C-D)[3(C+D) + \sqrt{8C^2 + (C+D)^2}]}{4D(2C+D)} \triangleq A_p. \end{aligned}$$

It is easy to prove that $0 < A_n < A_1 < A_2 < A_p < \frac{C-D}{D}$. Moreover, it follows from the existence condition of E_3 that

$$\frac{(C-D)E}{D} < A < \frac{C-D}{D} \Rightarrow E_H < \frac{AD}{C-D} \Leftrightarrow \frac{C-D}{C+D} < A < \frac{C-D}{D}.$$

Hence, the required constraints on A are given by

$$A \in (A_2, A_p),$$

for which $0 < E_H < \frac{1}{2}$.

To find the normal form (or focus value) of the system associated with the Hopf bifurcation, we multiply the equations in (19) by $A + X$ (i.e. applying a time rescaling $\tau \to (A+X)\tau$) for convenience, and then apply the following transformation,

$$X = \frac{AD}{C-D} + x_1, \quad Y = \left(1 - \frac{AD}{C-D}\right)\left(\frac{AD}{C-D} - E\right)\left(A + \frac{AD}{C-D}\right) - \frac{\omega_c(C-D)}{AD}x_2,$$

where

$$\omega_c = \frac{AC(C-D-AD)}{C-D}\sqrt{\frac{AD}{(C-D)[A(C+D)-(C-D)]}} > 0, \quad \text{for } A \in (A_2, A_p).$$

Applying the above transformation, we have the following new system:

$$\begin{aligned}\dot{x}_1 &= \omega_c x_2 - \frac{AD[A^2(C^2+CD+D^2) - A(C-D)(C+2D) + (C-D)^2]}{(C-D)^2[A(C+D)-(C-D)]}x_1^2 \\ &\quad + \frac{(C-D)\omega_c}{AD}x_1x_2 - \frac{A^2(C^2+2CD+2D^2) - A(C-D)(C+3D) + (C-D)^2}{(C-D)[A(C+D)-(C-D)]}x_1^3 - x_1^4, \\ \dot{x}_2 &= -\omega_c x_1 + (C-D)x_1x_2.\end{aligned}$$

Now, applying the Maple program [Yu, 1998] to the above system we obtain the following first-order focus value:

$$\begin{aligned}v_1 &= -\frac{1}{8(C-D)[A(C+D)-(C-D)]} \\ &\quad \times [(2C^2+5CD+5D^2)A^2 - (C-D) \\ &\quad \times (2C+7D)A + 2(C-D)^2],\end{aligned}$$

where the denominator in v_1 is positive for $A \in (A_2, A_p)$, and the term in the square bracket is a quadratic polynomial in A, which has the discriminant,

$$\Delta = -3(C-D)^2(2C+3D)(2C-D) < 0, \qquad (C > D),$$

implying that the term in the square bracket is positive and so $v_1 < 0$. Therefore, the codimension of the Hopf bifurcation is one, and it is supercritical, yielding stable limit cycles. ■

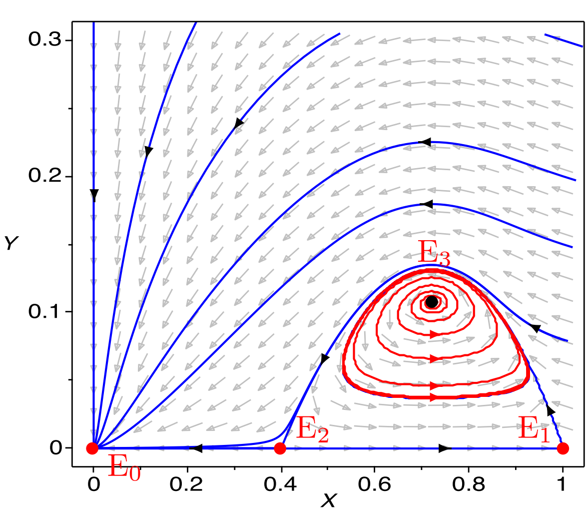

Fig. 5. Simulated phase portraits for model A_{ii} with $A = 0.48$, $C = 1$, $D = 0.6$, $E = 0.4$, showing bistable phenomenon — either converging to the stable equilibrium E_0 or to a stable limit cycle.

3.4. *Bifurcation diagram and simulation*

The bifurcation diagram of system A_{ii} for $C > D$ is shown in Fig. 4(b).

Because the simulations for this model A_{ii} are similar to that of the model A_1 (see Fig. 3), we only present the phase portraits near the Hopf critical point, see Fig. 4. For simulation, taking $C = 1$, $D = 0.6$, $E = 0.4$, we have

$$0.2667 \approx \frac{(C-D)E}{D} < A_{\mathrm{H}} = \frac{2}{195}(28+\sqrt{394}) \approx 0.4908 < \frac{C-D}{D} \approx 0.6667.$$

The simulation for $A = 0.48 < A_{\mathrm{H}}$ is depicted in Fig. 5 demonstrating the bistable phenomenon: trajectories either converge to the stable equilibrium E_0 or to a stable limit cycle, depending upon the initial conditions. This again shows an excellent agreement with the analytical prediction.

Remark 3.3. Comparing the bifurcation diagram in Fig. 4(b) having the Allee effect with that in Fig. 4(a) without the Allee effect shows the great impact of the Allee effect on the dynamics of system A_{ii}. Since system A_{ii} is quite similar to system A_i, Remark 2.3 on dynamics A_i can be applied here, as long as the three critical values in Fig. 2(a), $\frac{D}{C} = E$, $\frac{1+E}{2}$ and 1 are changed to $A = \frac{(C-D)E}{D}$, A_{H} and $\frac{C-D}{D}$, respectively. The bistable phenomenon with one stable equilibrium and one stable limit cycle is shown in Fig. 5.

4. Dynamics and Bifurcations of System B_i

We first summarize the results for the model without the Allee effect.

4.1. *The results for model* $\mathrm{B_i}$ *without the Allee effect*

The model without the Allee effect is described by

$$\begin{aligned}\dot{X} &= X(1-X) - MX,\\ \dot{Y} &= X - DY.\end{aligned} \tag{28}$$

which has only two equilibrium solutions, given below with stability [Jiang & Yu, 2017]:

$$\begin{aligned}&\mathrm{E_0} = (0,0), \quad \text{GAS for } M \geq 1,\\ &\mathrm{E_3} = \left(1-M, \frac{1-M}{D}\right), \quad \text{GAS for } 0 < M < 1,\end{aligned} \tag{29}$$

which clearly shows that the system does not have complex dynamical behaviors, but either a GAS equilibrium $\mathrm{E_0}$ or a GAS equilibrium $\mathrm{E_3}$ depending on whether $M \geq 1$ or $M < 1$. The bifurcation diagram is shown in Fig. 6(a).

4.2. *Stability and bifurcation of equilibria of system* $\mathrm{B_i}$ *with the Allee effect*

The model $\mathrm{B_i}$ with the Allee effect is described by

$$\mathrm{B_i}: \begin{cases}\dot{X} = X(1-X)(X-E) - MX \triangleq h_1(X),\\ \dot{Y} = X - DY \triangleq h_2(X,Y),\end{cases} \tag{30}$$

which also has only two equilibrium solutions, given below:

$$\begin{aligned}&\mathrm{E_0}: \ (X_0, Y_0) = (0,0),\\ &\mathrm{E_3}: \ (X_3, Y_3) = \left(X_3, \frac{1}{D}X_3\right),\end{aligned} \tag{31}$$

where X_3 is determined from the following quadratic polynomial equation,

$$\begin{aligned}F_1 &= (1-X_3)(X_3-E) - M\\ &= -[X_3^2 - (1+E)X_3 + E + M] = 0.\end{aligned} \tag{32}$$

The quadratic polynomial has two solutions:

$$\begin{aligned}X_{3\pm} &= \frac{1+E \pm \sqrt{\Delta_{\mathrm{B_i}}}}{2},\\ &\text{where } \Delta_{\mathrm{B_i}} = (1+E)^2 - 4(E+M)\\ &\qquad = (1-E)^2 - 4M.\end{aligned} \tag{33}$$

$\Delta_{\mathrm{B_i}} \geq 0$ is needed for $X_{3\pm}$ to be real positive, which yields

$$0 < M < \frac{(1-E)^2}{4} \triangleq M_{\mathrm{u}}. \tag{34}$$

It is easy to see that $E < X_{3\pm} < 1$ under the condition (34). When $M = M_{\mathrm{u}}$, $F = 0$ has a unique solution: $X_3 = \frac{1+E}{2} \in (E, 1)$, which actually defines a saddle-node bifurcation point. For $M > M_{\mathrm{u}}$, $\mathrm{E_3}$ does not exist. More precisely, define the equilibria:

$$\mathrm{E_{3\pm}} = \left(X_{3\pm}, \frac{1}{D}X_{3\pm}\right). \tag{35}$$

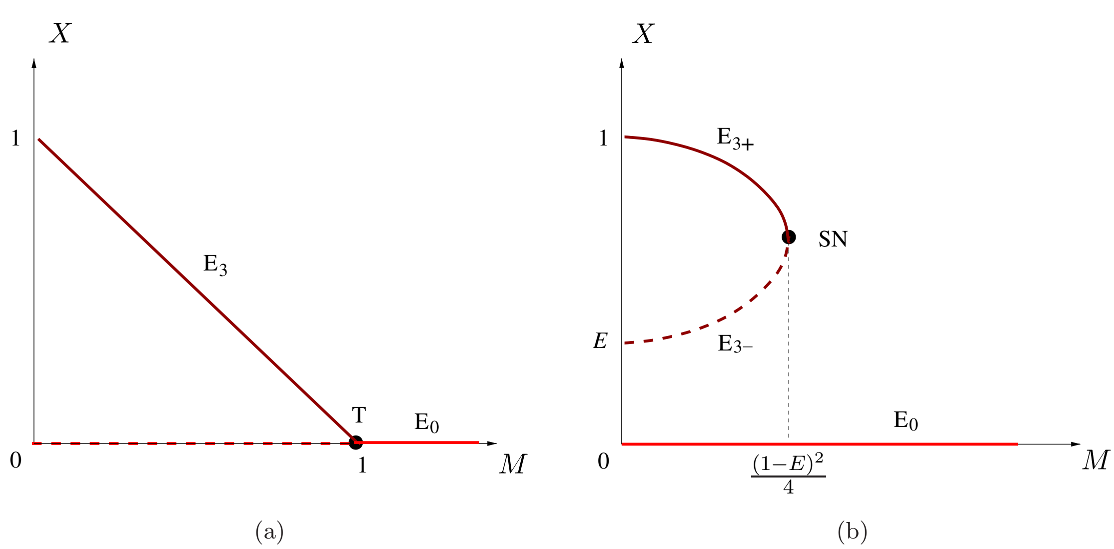

Fig. 6. Bifurcation diagrams for system $\mathrm{B_i}$: (a) without the Allee effect and (b) with the Allee effect.

For stability and bifurcation of the equilibria, we have the following theorem.

Theorem 4.1. *For the system* $\mathrm{B_i}$, $\mathrm{E_0}$ *is a stable node*; $\mathrm{E_{3-}}$ *is a saddle point, while* $\mathrm{E_{3+}}$ *is a stable focus. There is no Hopf bifurcation, nor B–T bifurcation.*

Proof. Note that equation $\dot{Y}$ is decoupled from equation $\dot{X}$, and that $\frac{\partial h_2}{\partial Y} = -D < 0$, which clearly shows that there is no Hopf bifurcation, nor B–T bifurcation. For stability of the equilibria, we only need to consider the equation $\dot{X}$, i.e. the function $h_1(X)$. It is easy to obtain

$$h_1'(X) = -E + 2(1+E)X - 3X^2 - M.$$

So $h_1'(0) = -(E+M) < 0$ indicates that $\mathrm{E_0}$ is a stable node.

Next, evaluating $h_1'(X_{3\pm})$ yields

$$h_1'(X_{3\pm}) = -\frac{1}{2}\sqrt{(1-E)^2 - 4M} \times [\sqrt{(1-E)^2 - 4M} \pm (1+E)]$$

and so $h_1'(X_{3-}) > 0$, implying that $\mathrm{E_{3-}}$ is a saddle point; while $h_1'(X_{3+}) < 0$, indicating that $\mathrm{E_{3+}}$ is a stable node. Moreover, at the turning point $M = M_{\mathrm{u}}$, $g_1'(X_{3\pm}) = 0$, we know that M_{u} is a saddle-node bifurcation point. ■

4.3. *Bifurcation diagram and simulation*

The bifurcation diagram is shown in Fig. 6(b).

The model $\mathrm{B_i}$ does not have Hopf bifurcation, but exhibits bistable phenomenon involving two stable equilibria, $\mathrm{E_0}$ and $\mathrm{E_3}$, which does not appear in the model without the Allee effect. To show the bistable phenomenon, we choose $D = 0.5$, $E = 0.25$ and $M = 0.10 < \frac{(1-E)^2}{4} = 0.140625$. The simulation is given in Fig. 7, which shows that trajectories either converge to the stable equilibrium $\mathrm{E_0}$ or to the equilibrium $\mathrm{E_3}$ depending on the initial conditions. Since the solution X_3 is independent of D (only depending upon E and M), and $Y_3 = \frac{X_3}{D}$ which yields $\frac{Y_3}{X_3} = \frac{1}{D}$, we see that Y_3 is monotonically increasing as D is decreasing regardless the value X_3.

Remark 4.2. It is seen from Figs. 6 and 7 that although this system does not have Hopf bifurcation, nor B–T bifurcation, the Allee effect does have an impact on the dynamics. In particular, the transcritical bifurcation is changed to a saddle-node bifurcation, and the unstable part of the equilibrium $\mathrm{E_0}$ without the Allee effect becomes stable with the Allee effect, which indicates an increase of extinction risk of species. Moreover, note that the equilibrium $\mathrm{E_3}$ exists with smaller interval in the parameter M for the system with the Allee effect [see Fig. 6(b)], compared to that without the Allee effect. Also note that the X-axis is no longer invariant for $\mathrm{B_i}$ system, as seen in Fig. 7, regardless whether the system has or does not have the Allee effect. However, the system still has the positivity property.

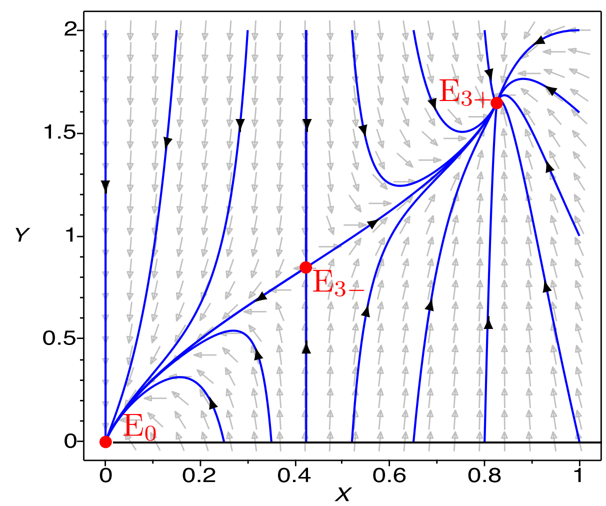

Fig. 7. Simulated phase portraits for the model $\mathrm{B_i}$ with $D = 0.5$, $E = 0.25$, $M = 0.1$, showing a bistable phenomenon, either converging to the stable equilibrium $\mathrm{E_0}$ or to the stable equilibrium $\mathrm{E_{3+}}$.

5. Dynamics and Bifurcations of System $\mathrm{B_{ii}}$

Finally, we consider system $\mathrm{B_{ii}}$. Again, we first list the existing results for the system without the Allee effect.

5.1. *The results for model* $\mathrm{B_{ii}}$ *without the Allee effect*

The system without the Allee effect is described by

$$\dot{X} = X(1-X) - \frac{MXY}{X+Y}, \qquad \dot{Y} = Y\left(\frac{CX}{X+Y} - D\right), \tag{36}$$

which has three equilibrium solutions given below together with stability [Jiang & Yu, 2017]:

$$\begin{aligned}
&\mathrm{E}_0 = (0,0), && \text{Stable or unstable or coexistence of stable and unstable sectors;}\\
&\mathrm{E}_1 = (1,0), && \text{GAS (a node) for } 0 < C \le D, \text{ and a saddle point for } C > D;\\
&\mathrm{E}_3 = \left(X_3, \left(\frac{C}{D} - 1\right) X_3\right), && \text{GAS for } 0 < M < \frac{C}{C-D}, \quad C \ge D+1,\\
& && \text{LAS for } 0 < M < \frac{C(C+DC-D^2)}{C^2-D^2}, \quad D < C < D+1,\\
& && \text{Supercritical Hopf bifurcation at } M = M_{\mathrm{H}} = \frac{C(C+DC-D^2)}{C^2-D^2},
\end{aligned} \tag{37}$$

where $X_3 = 1 - M(1 - \frac{D}{C})$. It should be noted that unlike the previous systems, the dynamics near the equilibrium E_0 in the first quadrant is very complex, and has been studied in detail by Xiao and Ruan [2001] using the blow-up technique. It was shown that in a neighborhood of E_0, there can exist various types of topological structures including the parabolic orbits, the elliptic orbits, the hyperbolic orbits, and any combination of them. In particular, E_0 can be asymptotically stable or unstable, or even coexistence of stable and unstable sectors.

For a comparison, the bifurcation diagrams for system (36) without the Allee effect are given in Figs. 8(a) and 8(b), in which only two cases $C \ge D+1$ and $D < C < D+1$ are shown, since the equilibrium E_1 is globally asymptotically stable for $0 < C \le D$.

5.2. *Stability and bifurcation of equilibria of system* $\mathrm{B_{ii}}$ *with the Allee effect*

The model $\mathrm{B_{ii}}$ with the Allee effect is given by

$$\mathrm{B_{ii}}: \begin{cases} \dot{X} = X(1-X)(X-E) - \dfrac{MXY}{X+Y}, \\[2mm] \dot{Y} = Y\left(\dfrac{CX}{X+Y} - D\right), \end{cases} \tag{38}$$

The system $\mathrm{B_{ii}}$ has four equilibrium solutions:

$$\begin{aligned}
&\mathrm{E}_0: (X_0, Y_0) = (0,0),\\
&\mathrm{E}_1: (X_1, Y_1) = (1,0),\\
&\mathrm{E}_2: (X_2, Y_2) = (E,0),\\
&\mathrm{E}_3: (X_3, Y_3) = \left(X_3, \frac{C-D}{D} X_3\right),
\end{aligned} \tag{39}$$

where X_3 is determined from the following quadratic polynomial equation:

$$F_{\mathrm{B_{ii}}} = X_3^2 - (1+E)X_3 + E + \frac{C-D}{C} M = 0, \tag{40}$$

which has solutions:

$$\begin{aligned}
X_{3\pm} &= \frac{1}{2}\left[(1+E) \pm \sqrt{(1+E)^2 - 4\left(E + \frac{(C-D)M}{C}\right)}\right]\\
&= \frac{1}{2}\left[(1+E) \pm \sqrt{(1-E)^2 - \frac{4(C-D)}{C}M}\right].
\end{aligned} \tag{41}$$

It is easy to see that $E < X_{3\pm} < 1$. Note that $C > D$ (required by $Y_3 > 0$) and $X_3 > 0$ are needed to guarantee that E_3 is an interior (positive) equilibrium. To have $X_3 > 0$, we require

$$\Delta_{\mathrm{B_{ii}}} = (1-E)^2 - \frac{4(C-D)}{C} M > 0.$$

Let

$$M_{\mathrm{u}} = \frac{C(1-E)^2}{4(C-D)}. \tag{42}$$

Then, $F_{\mathrm{B_{ii}}}$ has two real positive solutions when $0 < M < M_{\mathrm{u}}$ ($\Delta > 0$); one unique solution when $M = M_{\mathrm{u}}$; and no real solution when $M > M_{\mathrm{u}}$. Define

$$\mathrm{E}_{3\pm} = \left(X_{3\pm}, \frac{C-D}{D} X_{3\pm}\right). \tag{43}$$

For the stability of the equilibrium solutions, we have the following two theorems. The first one is for E_0. It should be noted that system (38) is not well defined at E_0. But since the X-axis and Y-axis are invariant, and so $\lim_{X\to 0^+, Y\to 0^+} \frac{XY}{X+Y} = \lim_{X\to 0^+, Y\to 0^+} \frac{1}{1/X+1/Y} = 0$ provided that $X > 0$, $Y > 0$. Thus, for system (38) we define that $\dot{X} = \dot{Y} = 0$ when $X = Y = 0$. However, the stability analysis of this equilibrium is not straightforward. We will again apply the blow-up technique to give a complete analysis on the stability of this equilibrium and show that, unlike E_0 of the system without the Allee effect, E_0 of the system with the Allee effect is actually a stable node. For convenience, define the region in the first quadrant (including the X-axis and Y-axis) in the X–Y plane as I and the interior of the first quadrant as I^+.

Theorem 5.1. *For system* B_{ii}, E_0 *is a stable node in* I^+.

Proof. First, it is easy to see from the equations in system (38) that both the X-axis and the Y-axis are invariant, and near E_0 trajectories converge to E_0 along the two axes. Thus, we only need to consider the solution trajectories in I^+.

In order to apply the blow-up technique, we introduce the time rescaling $d\tau = (X + Y)d\tau_1$ into (38) such that system (38) is equivalent to the following system in I^+ (where the dot is now used to indicate differentiation with respect to τ_1),

$$\overline{B}_{ii}: \begin{cases} \dot{X} = X(1-X)(X-E)(X+Y) - MXY \\ \quad = -MXY - EX(X+Y) \\ \quad\quad + X^2(X+Y)(1+E-X) \\ \quad \triangleq X_2(X,Y) + \Phi(X,Y), \\ \dot{Y} = CXY - DY(X+Y) \\ \quad \triangleq Y_2(X,Y), \end{cases} \tag{44}$$

where X_2 and Y_2 represent second-degree homogeneous polynomials in X and Y, and $\Phi(X,Y) = X^2(X+Y)(1+E-X)$. It is obvious that E_0 is an isolated critical point of higher order for the system (44).

It is easy to see that system (44) is analytic in a neighborhood of E_0. According to Theorem 3.10 in [Zhang *et al.*, 1991], any orbit of (44) tending to E_0 must tend it spirally or along a fixed direction, which is determined by the characteristic equation of system (44). Since the solution of (44) is restricted in I^+, it is impossible to have the possibility that the orbit of (44) tending to E_0 spirally, and the only possibility is tending to E_0 along a fixed direction.

Introduce the polar coordinates $X = r\cos\theta$, $Y = r\sin\theta$ into (44), and define

$$\begin{aligned} G(\theta) &= \cos\theta Y_2(\cos\theta,\sin\theta) - \sin\theta X_2(\cos\theta,\sin\theta) \\ &= \sin\theta\cos\theta[(C+E-D)\cos\theta \\ &\quad + (M+E-D)\sin\theta], \\ H(\theta) &= \sin\theta Y_2(\cos\theta,\sin\theta) + \cos\theta X_2(\cos\theta,\sin\theta) \\ &= -\sin^2\theta[D\sin\theta + (D-C)\cos\theta] \\ &\quad - \cos^2\theta[E\cos\theta + (M+E)\sin\theta], \end{aligned} \tag{45}$$

where $\theta \in (0, \frac{\pi}{2})$. The characteristic equation of (44) takes the form $G(\theta) = 0$, which clearly shows that this equation either has a real root θ_1 or $G(\theta) \equiv 0$ in $\theta \in (0, \frac{\pi}{2})$. In order to apply Theorems 3.1–3.3 in [Zhang *et al.*, 1991], based on $G(\theta)$, we consider the following four cases:

(i) $C + E - D = 0$, $M + E - D \neq 0$, for which we have

$$G(\theta) = \sin^2\theta\cos\theta(M+E-D) \neq 0 \quad \text{for } \theta \in \left(0, \frac{\pi}{2}\right).$$

(ii) $C + E - D \neq 0$, $M + E - D = 0$, which yields

$$G(\theta) = \sin\theta\cos^2\theta(C+E-D) \neq 0 \quad \text{for } \theta \in \left(0, \frac{\pi}{2}\right).$$

(iii) $(C + E - D)(M + E - D) \neq 0$, for which we obtain

$$G(\theta) = \sin\theta\cos^2\theta(M+E-D) \times \left[\tan\theta + \frac{C+E-D}{M+E-D}\right],$$

which further gives two subcases:

(iii-a) $(C + E - D)(M + E - D) > 0$, leading to either $C > D - E$, $M > D - E$, or $C < D - E$, $M < D - E$ $(D > E)$, both yield

$$G(\theta) \neq 0 \quad \text{for } \theta \in \left(0, \frac{\pi}{2}\right).$$

(iii-b) $(C+E-D)(M+E-D) < 0$ (i.e. $C < D-E < M$ or $M < D-E < C$, $D > E$), for which we have a uniqure solution θ_1 such that

$G(\theta_1) = 0$, where

$$\theta_1 = \tan^{-1}\left[\frac{-(C+E-D)}{M+E-D}\right] \in \left(0, \frac{\pi}{2}\right).$$

(iv) $(C+E-D) = (M+E-D) = 0$ which yields $C = M = D-E$ $(D > E)$ under which

$$G(\theta) \equiv 0.$$

This is a singular case. Using the Briot–Bouquet transformation $Y = uX$ (and so $u > 0$ due to $X, Y > 0$), (44) can be changed to [Zhang *et al.*, 1991]

$$\begin{aligned}\frac{du}{dX} &= \frac{-u\Phi^*(X,u)}{X_2(1,u) + X\Phi^*(X,u)} \\ &= \frac{u(1+u)(E+1-X)}{u(D-E) + (1+u)(1-X)(E-X)} \\ &\triangleq g(u,X), \end{aligned} \tag{46}$$

where

$$X_2(1,u) = \frac{\Phi(X,uX)}{X^2} = -(Du+E) < 0,$$

$$\Phi^*(X,u) = \frac{\Phi(X,uX)}{X^3} = (1+u)(1+E-X).$$

Hence, according to [Zhang *et al.*, 1991], on the (X,Y)-plane, there exists a direction $\theta = \theta_1^*$ along which an orbit of (44) tends to E_0 if and only if there is a solution curve of (46) passing through the point $(0, u_1^*)$ on the (X,u)-plane, with $u_1^* = \tan\theta_1^*$. For $0 < X \ll 1$ and $u > 0$, we have the continuous function $g(u,X) > 0$ and the continuous function,

$$\frac{\partial g(u,X)}{\partial u} = \frac{(1+E-X)[E + 2Eu + Du^2 - (1+E)(u+1)^2X + (1+u)^2X^2]}{[u(D-E) + (1+u)(1-X)(E-X)]^2} > 0,$$

because

$$\begin{aligned} &E + 2Eu + Du^2 - (1+E)(u+1)^2X + (1+u)^2X^2 \\ &\quad > (1+u)^2(1-X)(E-X) \\ &\quad > 0 \quad \text{for } 0 < X \ll 1, \end{aligned}$$

due to $D > E$. This shows that the differential equation (46) has a unique solution passing through the point $(0, u_1^*)$, $u_1^* > 0$, implying that on the (X,Y)-plane, for any $\theta_1^* \in (0, \frac{\pi}{2})$, there exists a unique trajectory tending to E_0 along the direction $\theta = \theta_1^*$.

Next, we investigate the direction that the orbit moves along $\theta = \theta_1$ (for the case (iii-b)) and $\theta = \theta_1^*$ (for the case (iv)). To achieve this, using the polar coordinates, the system (38) can be transformed to (neglecting higher order terms)

$$\dot{r} = \frac{rH(\theta)}{\sin\theta + \cos\theta}, \quad \dot{\theta} = \frac{G(\theta)}{\sin\theta + \cos\theta}. \tag{47}$$

Then, for the case (iii-b), using $G(\theta) = 0$ and the unique solution $\tan\theta_1 = -\frac{C+E-D}{M+E-D}$, we obtain

$$\begin{aligned} H(\theta_1) &= -\sin^2\theta_1[D\sin\theta_1 + (D-C)\cos\theta_1] \\ &\quad - \cos^2\theta_1[D\sin\theta_1 + (D-C)\cos\theta_1] \\ &= -[D - C + D\tan\theta_1]\cos\theta_1 \\ &= -\frac{(D-C)M - CE}{M+E-D}\cos\theta_1 \\ &= \frac{(C-D)M + CE}{M+E-D}\cos\theta_1. \end{aligned}$$

Thus, for $C < D-E < M$, we have $M+E-D > 0$ and $(D-C)M - CE > E(M-C) > 0$; while for $M < D-E < C$ $(D > E)$, we have $M+E-D < 0$ and $(C-D)M + CE > E(C-M) > 0$. Hence, the orbit moves towards E_0 in the direction $\theta = \theta_1$ for the case (iii-b).

For the case (iv), it is known that $\theta_1^* \in (0, \frac{\pi}{2})$. Using the condition $C = M = D-E$ $(D > E)$, we obtain

$$\begin{aligned} H(\theta_1^*) &= -\sin^2\theta_1^*(D\sin\theta_1^* + E\cos\theta_1^*) \\ &\quad - \cos^2\theta_1^*(E\sin\theta_1^* + D\cos\theta_1^*) \\ &= -(\sin\theta_1^* + \cos\theta_1^*)[D(1 - \sin\theta_1^*\cos\theta_1^*) \\ &\quad + E\sin\theta_1^*\cos\theta_1^*] \\ &< 0 \quad \text{for } \theta_1^* \in \left(0, \frac{\pi}{2}\right). \end{aligned}$$

Summarizing the above discussions we have shown that including the X-axis and the Y-axis, orbits move towards E_0 along the characteristic direction in the neighborhood of E_0 in the first quadrant of the (X, Y)-plane as $t \to +\infty$.

The proof of Theorem 5.1 is complete. ■

Remark 5.2. The Allee effect has significant influence on the equilibrium E_0. Without the Allee effect, it has been shown that as the parameter varied, the dynamics of the system around E_0 in the first quadrant of the phase portrait can be very complex [Xiao & Ruan, 2001]. It can be stable or unstable, and even for the same set of parameter values, it can be stable or unstable depending upon the initial values. However, for system (38) with the Allee effect, E_0 becomes always stable, at least locally, which again indicates an increase of extinction risk of species.

Theorem 5.3. *For system* B_{ii}, E_1 *is either a stable node if* $C < D$, *or a saddle point if* $C > D$; E_2 *is unstable* (*either a saddle point when* $C < D$, *or an unstable node when* $C > D$). $E_{3\pm}$ *exist for* $0 < M < M_u$, *and* E_{3-} *is always a saddle point.* E_{3+} *is a stable focus for* $C \geq D + \frac{(1-E)^2}{4}$, *and for* $D < C < D + \frac{(1-E)^2}{4}$ *if* $0 < M < M_H$; E_{3+} *is an unstable focus for* $D < C < D + \frac{(1-E)^2}{4}$ *if* $M_H < M < M_u$. *Hopf bifurcation occurs from* E_{3+} *at the critical point* $M = M_H$, *where* M_H *is given by*

$$M_H = \frac{C}{2(C-D)(2C+D)^2}\{(2C+D)[2D(C-D)+C(1-E)^2] - C^2(1+E)^2 + C(1+E)\sqrt{C^2(1+E)^2 + D(2C+D)[(1-E)^2 - 4(C-D)]}\}. \tag{48}$$

Proof. To study the stability of the equilibria, we calculate the Jacobian of system (38), given by

$$J(X,Y) = \begin{bmatrix} -E + 2(1+E)X - 3X^2 - \dfrac{MY^2}{(X+Y)^2} & -\dfrac{MX^2}{(X+Y)^2} \\ \dfrac{CY^2}{(X+Y)^2} & \dfrac{CX^2}{(X+Y)^2} - D \end{bmatrix}. \tag{49}$$

Evaluating the J on the equilibrium E_1, we have two eigenvalues $-(1-E) < 0$ and $C - D$. Hence, E_1 is a stable node if $C < D$ or a saddle point if $C > D$. For the equilibrium E_2, we obtain two eigenvalues $E(1-E) > 0$ and $C - D$, which implies that E_2 is a saddle point if $C < D$ or an unstable node if $C > D$.

For the positive equilibria $E_{3\pm}$, we compute the J on $E_{3\pm}$ to obtain the determinant:

$$\det(J(E_{3\pm})) = \frac{D(C-D)}{2C}\sqrt{(1-E)^2 - 4M\left(1 - \frac{D}{C}\right)} \times \left[\sqrt{(1-E)^2 - 4M\left(1-\frac{D}{C}\right)} \pm (1+E)\right], \tag{50}$$

yielding $\det(J(E_{3-})) < 0$ and $\det(J(E_{3+})) > 0$. Thus, the equilibrium E_{3-} is a saddle point, and the stability of E_{3+} is determined by the sign of $\mathrm{Tr}(J(E_{3+}))$: E_{3+} is asymptotically stable if $\mathrm{Tr}(J(E_{3+})) < 0$ and unstable if $\mathrm{Tr}(J(E_{3+})) > 0$. A direct computation shows that

$$\mathrm{Tr}(J(E_{3+})) = -\frac{1}{2C^2} f_2,$$

where f_2 is given by

$$f_2 = 2D(C-D)(C-M) + C[C(1-E)^2 - 4M(C-D)] + C(1+E)\sqrt{C[C(1-E)^2 - 4M(C-D)]}, \tag{51}$$

for which $0 < M < M_u = \frac{C(1-E)^2}{4(C-D)}$ and so the second and third terms in f_2 are positive, implying that $f_2 \gtrless 0 \Leftrightarrow \mathrm{Tr}(J(E_{3+})) \lessgtr 0$. In the following, we discuss the sign of f_2, which has several cases.

(I) $0 < M \leq C$ for which $f_2 > 0 \Leftrightarrow \mathrm{Tr}(J(E_{3+})) < 0$ and so E_{3+} is asymptotically stable. Comparing M with the limiting value M_u, we have two subcases:

(Ia) If $C \geq M_u$, i.e. $C \geq D + \frac{(1-E)^2}{4}$, then E_{3+} is asymptotically stable for $0 < M < M_u$.

(Ib) If $C < M_{\rm u}$, i.e. $D < C < D + \frac{(1-E)^2}{4}$, then E_{3+} is asymptotically stable for $0 < M \leq C$.

(II) $M > C$ for which we consider the frist two terms in f_2 and define

$$M^* = \frac{C[C(1-E)^2 + 2D(C-D)]}{2(C-D)(2C+D)}. \tag{52}$$

Then, the first two terms in f_2 yield a positive value for $0 < M < M^*$ and a negative value for $M^* < M < M_{\rm u}$. In addition, it needs $M^* < M_{\rm u}$, leading to

$$\begin{aligned} M^* - M_u &= \frac{C[C(1-E)^2 + 2D(C-D)]}{2(C-D)(2C+D)} \\ &\quad - \frac{C(1-E)^2}{4(C-D)} \\ &= \frac{CD}{(C-D)(2C+D)} \\ &\quad \times \left[C - D - \frac{(1-E)^2}{4}\right] < 0, \end{aligned}$$

which implies that $D < C < D + \frac{(1-E)^2}{4}$. Note that

$$C < D + \frac{(1-E)^2}{4} \Leftrightarrow C < \frac{C(1-E)^2}{4(C-D)} = M_{\rm u}.$$

(IIa) If $0 < M < M^*$, we have $f_2 > 0$ and so E_{3+} is asymptotically stable.

(IIb) If $M^* < M < M_u$, the sum of the first two terms in f_2 becomes negative, so $f_2 \gtrless 0 \Leftrightarrow f_3 \gtrless 0$, where

$$\begin{aligned} f_3 &= C^3(1+E)^2[C(1-E)^2 - 4M(C-D)] \\ &\quad - \{2D(C-D)(M-C) \\ &\quad - C[C(1-E)^2 - 4M(C-D)]\}^2 \\ &= -4(C-D)^2(2C+D)^2M^2 + 4C(C-D) \\ &\quad \times \{(2C+D)[2D(C-D) + C(1-E)^2] \\ &\quad - C^2(1+E)^2\}M - 4C^2[D(C-D) \\ &\quad + C(1-E)][D(C-D) - CE(1-E)], \end{aligned}$$

which is a quadratic polynomial in M, having the following discriminant:

$$\begin{aligned} \Delta_{\rm B_{ii}} &= 16C^4(C-D)^2(1+E)^2\{C^2(1+E)^2 \\ &\quad + D(2C+D)[(1-E)^2 - 4(C-D)]\} \\ &> 0. \end{aligned}$$

So $f_3 = 0$ has two real solutions. Moreover, we have

$$\begin{aligned} f_3|_{M=M^*} &= \frac{DC^4(1+E)^2}{2C+D}[(1-E)^2 - 4(C-D)] \\ &> 0, \end{aligned}$$

due to $C < D + \frac{(1-E)^2}{4}$, and

$$f_3|_{M=M_u} = -\frac{D^2C^2}{4}[(1-E)^2 - 4(C-D)]^2 < 0.$$

Since f_3 is a quadratic polynomial in M with a negative coefficient of the term M^2 (implying that f_3 has a maximum), it must have a unique positive root $M = M_{\rm H} \in (M^*, M_u)$, where $M_{\rm H}$ is given in (48), which is the bigger one of the two real solutions. This solution yields $f_2 = 0$ and so $\mathrm{Tr}(J(\mathrm{E}_{3+})) = 0$, indicating that $M_{\rm H}$ is a Hopf critical point. Note that the other real root of f_3 does not satisfy $f_2 = 0$ and so it is not a Hopf critical point.

Summarizing the above discussions, we have the following results.

(1) When $C \geq D + \frac{(1-E)^2}{4}$, E_{3+} is asymptotically stable for $0 < M < M_{\rm u}$.
(2) When $D < C < D + \frac{(1-E)^2}{4}$, one of the following holds:
   (2-a) E_{3+} is asymptotically stable for $0 < M < M_{\rm H}$;
   (2-b) E_{3+} is unstable for $M_{\rm H} < M < M_{\rm u}$; and
   (2-c) Hopf bifurcation occurs from E_{3+} at the critical point $M = M_{\rm H}$. ■

5.3. *Codimension of the Hopf bifurcation*

Next, we further study the Hopf bifurcation and determine the codimension of the bifurcation. We have the following result.

Theorem 5.4. *For system* $\mathrm{B_{ii}}$, *Hopf bifurcation occurs from* E_{3+} *at the critical point* $M = M_{\rm H}$, *and the bifurcation is subcritical with codimension one, yielding a family of unstable limit cycles.*

Proof. Again we apply normal form theory to find the focus values to determine the stability of limit cycles. To achieve this and make it simpler in normal form computation, we solve the equation in (40) for C, instead of solving for X_3, to obtain (noticing that in the following $X_3 = X_{3+}$)

$$C = \frac{MD}{M-(1-X_3)(X_3-E)} > 0$$
$$\Rightarrow M > (1-X_3)(X_3-E) > 0,$$
$$(E < X_3 < 1)$$

and then solving $\mathrm{Tr}(J(\mathrm{E}_3))$ for M yields the Hopf critical point, given by

$$M_{\mathrm{H}} = \frac{(1-X_3)(X_3-E)[D+(X_3-E)(1-X_3)]}{-3X_3^2+2(1+E)X_3-E} > 0,$$

which requires

$$-3X_3^2+2(1+E)X_3-E > 0,$$

and so

$$E < X_3 < \frac{1}{3}(1+E+\sqrt{1-E+E^2}) < 1, \quad \left(0 < E < \frac{1}{2}\right).$$

Then, we multiply the vector field of (38) by $X+Y$ for convenience (equivalent to using a time scaling, $\tau \to (X+Y)\tau$), and apply the following transformation at the critical point $M = M_{\mathrm{H}}$,

$$\begin{aligned} X &= X_3 + x_1, \\ Y &= \frac{C-D}{D}X_3 + \frac{D[(2X_3-E)(1-X_3)-X_3(X_3-E)]^2}{[D-(1+E)X_3+2X_3^2]^2(1-X_3)(X_3-E)}x_1 \\ &\quad - \frac{\omega_c[(2X_3-E)(1-X_3)-X_3(X_3-E)]}{X_3[D-(1+E)X_3+2X_3^2](1-X_3)(X_3-E)}x_2, \end{aligned} \tag{53}$$

where

$$\omega_c = \frac{X_3\sqrt{DX_3(2X_3-1-E)[D+(1-X_3)(X_3-E)][-3X_3^2+2(1+E)X_3-E]}}{|D+X_3(2X_3-1-E)|}.$$

In order to have $\omega_c > 0$, we need $X_3 > \frac{1}{2}(1+E)$. Since $M_{\mathrm{H}} < M_{\mathrm{u}}$, and noticing from (41) that $X_3 = \frac{1}{2}(1+E)$ at $M = M_{\mathrm{u}}$, we have $X_3 = X_{3+} > \frac{1}{2}(1+E)$ at $M = M_{\mathrm{H}}$. Therefore, we finally obtain

$$\frac{1}{2}(1+E) < X_3 < \frac{1}{3}(1+E+\sqrt{1-E+E^2}), \quad 0 < E < \frac{1}{2}. \tag{54}$$

Now, substituting the transformation (53) into system (38) with the time scaling, we obtain

$$\dot{x}_1 = \omega_c x_2 + \sum_{i+j=2}^{4} a_{ij}x_1^i x_2^j,$$
$$\dot{x}_2 = -\omega_c x_1 + \sum_{i+j=2}^{4} b_{ij}x_1^i x_2^j,$$

where a_{ij} and b_{ij} are coefficients in terms of D, E and X_3. Then, applying the Maple program [Yu, 1998] to the above system yields the following first-order focus value:

$$v_1 = \frac{G_1}{8X_3[D+X_3(2X_3-1-E)](2X_3-1-E)(X_3-E)(1-X_3)},$$

where

$$\begin{aligned} G_1 &= D(1+E)(1-X_3)(X_3-E) + G_2, \\ G_2 &= (1-E)^4X_3 - (1-X_3)(X_3-E)G_3, \\ G_3 &= (1-E)^2(10X_3-1-E) - (1-X_3)(X_3-E)(24X_3-3-3E). \end{aligned}$$

In the following, we prove $G_2 > 0$ and so $v_1 > 0$ for X_3 in the interval given in (54). First we show $G_3 > 0$. To simplify the analysis, we let $X_3 = \frac{1}{2}(1+E) + G$ and thus (54) is changed to

$$0 < G < G_{\mathrm{u}} = \frac{1}{6}[2\sqrt{1-E+E^2} - (1+E)] < \frac{1}{6}, \quad \text{for } E \in \left(0, \frac{1}{2}\right), \tag{55}$$

under which G_3 becomes

$$G_3 = 24G^3 + 9(1+E)G^2 + 4(1-E)^2G + \frac{7}{4}(1+E)(1-E)^2 > 0.$$

To prove $G_2 > 0$ in the region on the E–G plane, bounded by $0 < G < G_{\mathrm{u}}$, $0 < E < \frac{1}{2}$, we first show that the function G_2 has no extreme points inside the region and then prove that $G_2 > 0$ on the boundaries of the region. Now, G_2 is a function of G and E, given by

$$G_2(G,E) = \frac{1}{16}(1+E)(1-E)^4 - \frac{1}{2}G^2\{(1+E)(1-E)^2 + 2G[2(1-E)^2 - 3G(3E+8G+3)]\}$$

from which we obtain

$$\frac{\partial G_2}{\partial G} = -Gg_1, \quad \frac{\partial G_2}{\partial E} = -\frac{1}{16}(2G+1-E)g_2,$$

where

$$g_1 = (1+E)(1-E)^2 + 6G[(1-E)^2 - 2G(3E+10G+3)],$$
$$g_2 = (3+5E)(1-E)^2 - 2G[(3+5E) \times (1-E) + 2G(18G-1+E)].$$

Now with the help of Maple, eliminating G from the two equations $g_1 = 0$ and $g_2 = 0$ we obtain the solution,

$$G = \frac{(1-E)(220+527E+236E^2-11E^3)}{56+77E+124E^2+67E^3} > \frac{481}{238} > G_u, \quad E \in \left(0, \frac{1}{2}\right)$$

and a resultant,

$$\mathrm{R} = -(1-E)(1915E^5 + 677E^4 + 1390E^3 + 5978E^2 + 4615E + 977) < 0, \quad E \in \left(0, \frac{1}{2}\right),$$

which implies that $\frac{\partial G_2}{\partial G} = \frac{\partial G_2}{\partial E} = 0$ do not have solutions for $0 < E < \frac{1}{2}$, $0 < G < G_u$, and so the function G_2 does not have extreme points in the region bounded by $0 < E < \frac{1}{2}$ and $0 < G < G_u$.

Next, we prove that $G_2 > 0$ on the boundaries of the region, $0 < E < \frac{1}{2}$, $0 < G < G_u$, which has three line segments and one curve:

$$\mathrm{L}_1: \; E = 0, \quad 0 < G < \frac{1}{6},$$

$$\mathrm{L}_2: \; E = \frac{1}{2}, \quad 0 < G < \frac{\sqrt{3}}{12}(2-\sqrt{3}),$$

$$\mathrm{L}_3: \; G = 0, \quad 0 < E < \frac{1}{2},$$

$$\mathrm{C}_1: \; G = G_{\mathrm{u}}, \quad 0 < E < \frac{1}{2}.$$

By a direct computation, we obtain the following results.

$$\begin{aligned}
\text{On } \mathrm{L}_1: \; G_2(G,0) &= \frac{1}{16}(2G+1)(192G^4 - 24G^3 - 4G^2 - 2G + 1) \\
&= \frac{1}{16}(2G+1)[(1-6G)(1+4G+20G^2) + 96G^3 + 192G^4] \\
&> 0, \quad \text{for } 0 < G < \frac{1}{6}; \\
\text{On } \mathrm{L}_2: \; G_2\left(G, \frac{1}{2}\right) &= \frac{3}{512} - \frac{3}{16}G^2 - \frac{1}{2}G^3 + \frac{27}{2}G^4 + 24G^5 \\
&= \frac{3}{512}(1-20G)(1+20G+368G^2) + \frac{341}{8}G^3 + \frac{27}{2}G^4 + 24G^5 \\
&> 0, \quad \text{for } 0 < G < \frac{\sqrt{3}}{12}(2-\sqrt{3}) < \frac{1}{20}; \\
\text{On } \mathrm{L}_3: \; G_2(0,E) &= \frac{1}{16}(1+E)(1-E)^4 > 0, \quad \text{for } 0 < E < \frac{1}{2}.
\end{aligned}$$

On the curve C_1, we have

$$\begin{aligned} G(G_u, E) &= \frac{1}{81}(1+E)[(2E^4 - 7E^3 + 18E^2 - 7E + 2) + 2(E^2 - 4E + 1)(1+E)\sqrt{1 - E + E^2}] \\ &= \frac{1}{81}(1+E)\left[2\left(1 - \frac{7}{4}E\right)^2 + \frac{95}{8}E^2\left(1 - \frac{28}{95}E\right)^2 + \frac{92}{95}E^4\right. \\ &\quad \left. + 2(E^2 - 4E + 1)(1+E)\sqrt{1 - E + E^2}\right] \\ &= \frac{E^2(1+E)(1-E)^4}{\left\{\left[2\left(1 - \frac{7}{4}E\right)^2 + \frac{95}{8}E^2\left(1 - \frac{28}{95}E\right)^2 + \frac{92}{95}E^4 2(E^2 - 4E + 1)(1+E)\sqrt{1 - E + E^2}\right]\right\}}. \end{aligned}$$

Thus, $G(G_u, E) > 0$ regardless whether $E^2 - 4E + 1$ is positive or negative.

Therefore, by continuity of the function, $G_2 > 0$ on the region defined by (54), and so $v_1 > 0$, indicating that the codimension of the Hopf bifurcation is one, and it is subcritical with unstable bifurcating limit cycles. ■

5.4. *Bifurcation diagram and simulation*

The bifurcation diagrams are shown in Figs. 8(c) and 8(d), where only the cases for $C > D$ are presented, since for $C \le D$, E_1 is globally asymptotically stable, and E_3 does not exist.

Remark 5.5. Comparing the bifurcation diagrams in Fig. 8, it can be seen that the model B_{ii} with the Allee effect and without the Allee effect has similar dynamical behaviors. Both of them have Hopf bifurcation but the bifurcation curve changes from linear to nonlinear. Also note that the model with the Allee effect has less stable interval in M. The big difference is that the Hopf bifurcation for the model without the Allee effect is supercritical with stable limit cycles while that for the model with the Allee effect is subcritical with unstable limit cycles. Thus, the model without the Allee effect might have bistable phenomenon (containing one stable equilibrium and one stable limit cycle) if E_0 happens to be stable, while the model with the Allee effect does not have such bistable property. But the model with the Allee effect exhibits the bistable phenomenon with two equilibria E_0 and E_{3+}, see Figs. 8(c) and 8(d).

Now we present simulations for model B_{ii}. To have a comparison, we show simulations for both with and without the Allee effect. For the case without the Allee effect, it is seen from (37) that a supercritical Hopf bifurcation occurs from the critical point $M_H = \frac{C(C+DC-D^2)}{C^2-D^2}$ when $C \in (D, 1+D)$ [see Fig. 8(b)]. Let $D = 0.8$ and $C = 1$. Then $M_H = \frac{29}{9} \approx 3.22222222$, and $\frac{C}{C-D} = 5$. We take three values for simulation: $M = 3.224, 3.24133419, 3.24133420 > M_H$, which implies that the equilibrium E_{3+} is an unstable focus for the three values of M. The simulations given in Figs. 9(a)–9(f) show very different behaviors though the three values are very close to M_H. It is seen that the simulation for $M = 3.224$, as depicted in Figs. 9(a) and 9(b), shows a regular oscillation, while that for $M = 3.24133419$ shows a recurrence behavior [Zhang *et al.*, 2013, 2014; Yu *et al.*, 2016; Yu & Zhang, 2019], see Figs. 9(c) and 9(d), where the trajectory does not touch the equilibrium E_0 since E_0 is unstable. However, it is noted that the sufficient conditions given in the above mentioned articles do not include the case as seen in Figs. 9(c) and 9(d), since here the system does not exhibit saddle-node bifurcation or transcritical bifurcation.

It is interesting to see from the simulation, as given in Figs. 9(e) and 9(f), that when M has a very small increase from 3.24133419 to 3.24133420, the limit cycle (recurrent oscillation) disappears and the trajectory converges to the equilibrium E_0. According to the analysis in [Xiao & Ruan, 2001], the above three sets of parameter values belong to the category $D < C < 1+D < M_H < M < \frac{C}{C-D}$ for which the equilibrium E_0 can be either asymptotically stable or unstable, as shown in Fig. 10. It can

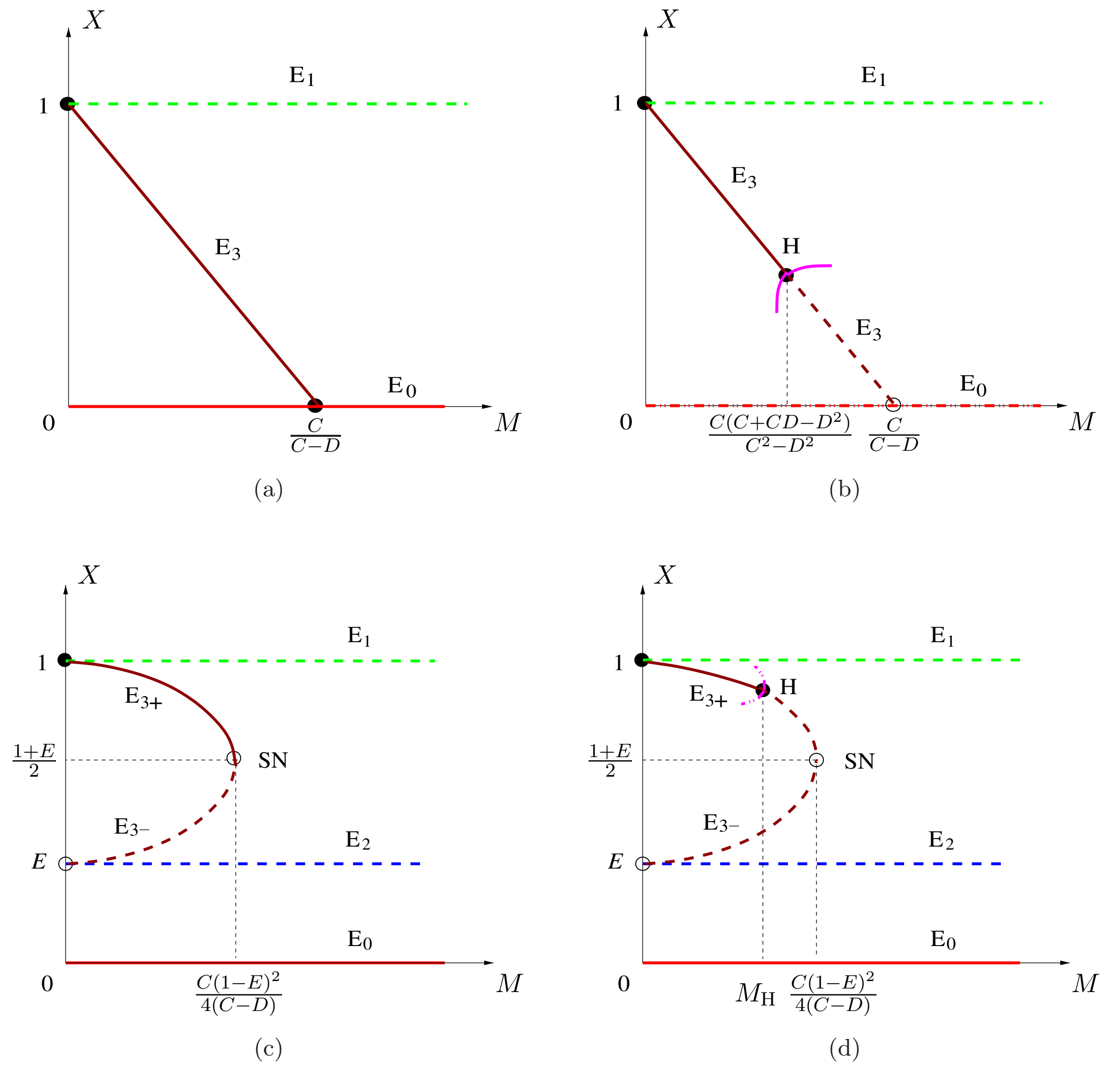

Fig. 8. Bifurcation diagram for system B_{ii} without the Allee effect: (a) for $C \geq 1 + D$, and (b) for $D < C < 1 + D$; and with the Allee effect: (c) for $C \geq D + \frac{(1-E)^2}{4}$ and (d) for $D < C < D + \frac{(1-E)^2}{4}$. The pink curves denote Hopf bifurcation, with solid (dashed) curve for supercritical (subcritical) Hopf bifurcation.

be seen from this figure that in the vicinity of the origin trajectories converge to the origin if $\theta > \theta^*$ while diverge from the origin if $\theta < \theta^*$. For the numerical values chosen for this example, we have $\theta^* = \tan^{-1} 0.555 = 29.03°$. This value 0.555 agrees with the slope of the trajectory near the origin, $\frac{0.01}{0.2/11} \approx 0.55$, see Figs. 9(c) and 9(e). It is expected that there exists a value of M between M_{H} and $\frac{C}{C-D}$ and close to M_{H}, at which the oscillation suddenly ceases. But such a critical value M^* cannot be analytically determined. Here, for the system (36) with $D = 0.8$ and $C = 1$, $M^* \approx 3.24133419$. So when $M_{\mathrm{H}} < M \leq M^*$, the trajectory starting from E_1 does not touch E_0 (the origin), and returns following a route below the blue curve [see Figs. 9(c) and 10] and converges to a stable limit cycle; while when $M > M^*$, the trajectory starting from E_1 converges to the origin following a route above the blue curve [see Figs. 9(e) and 10]. The critical value of M and the critical angle θ^* must be inherently related, yielding the interesting relaxation oscillation. This needs a further study.

It is seen from the bifurcation diagrams in Figs. 8(c) and 8(d) for model B_{ii} with the Allee effect that there exist two cases: either the system has no Hopf bifurcation if $C \geq D + \frac{(1-E)^2}{4}$, or Hopf bifurcation occurs from E_{3+} at the critical point $M = M_{\mathrm{H}}$ if $D < C < D + \frac{(1-E)^2}{4}$. The codimension of the Hopf bifurcation is one and it is subcritical, and so the bifurcating limit cycle is unstable. For

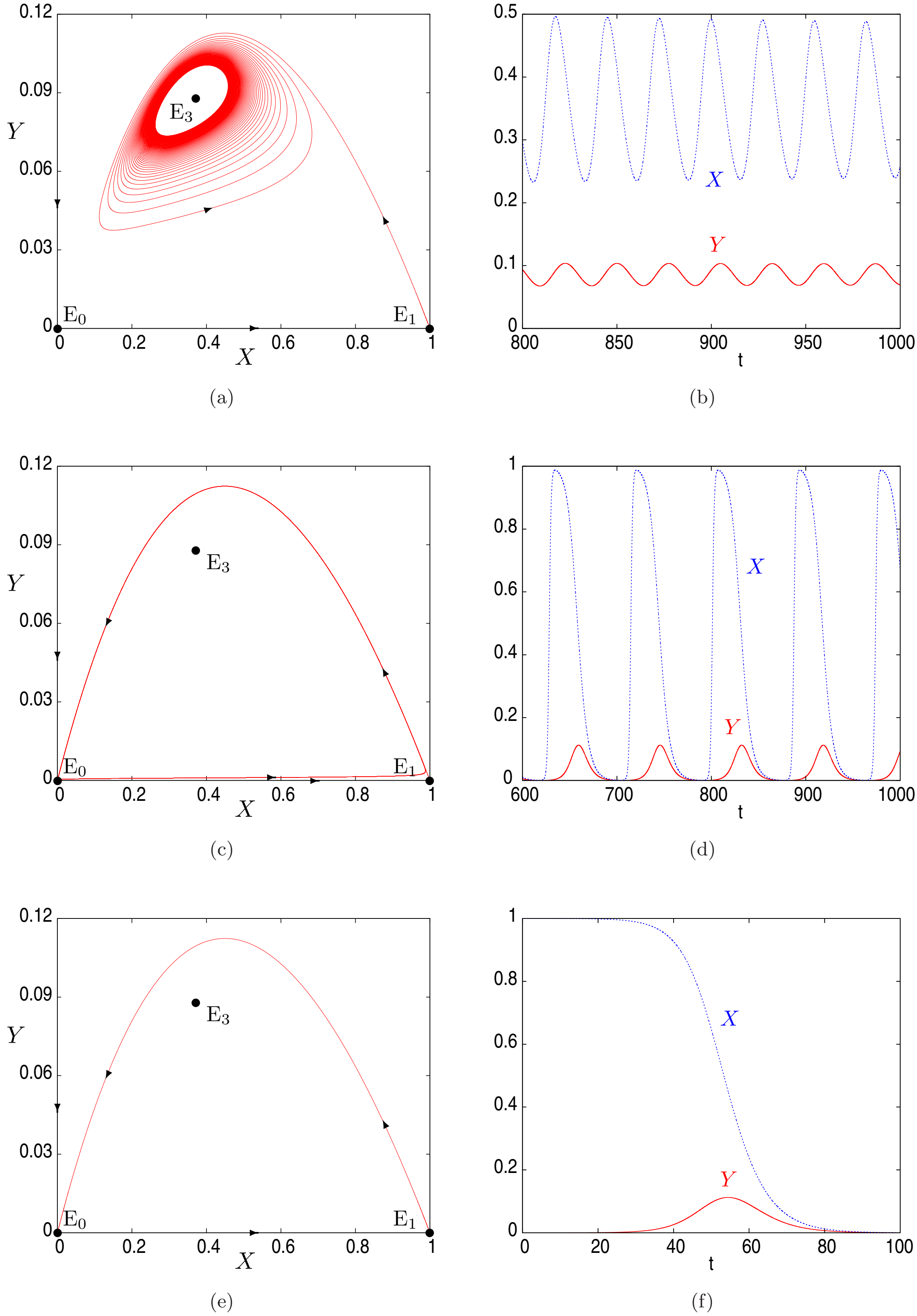

Fig. 9. Simulations for the $\mathrm{B_{ii}}$ model (36) without the Allee effect with $D = 0.8$, $C = 1$, starting from the initial point $(X, Y) = (1, 0.00001)$: (a) phase portrait for $M = 3.224$, and (b) time history for $M = 3.224$, showing a regular oscillation; (c) phase portrait for $M = 3.24133419$, and (d) time history for $M = 3.24133419$, showing a recurrent behavior (a slow-fast motion); (e) phase portrait for $M = 3.24133420$, and (f) time history for $M = 3.24133420$, showing convergence to the equilibrium E_0.

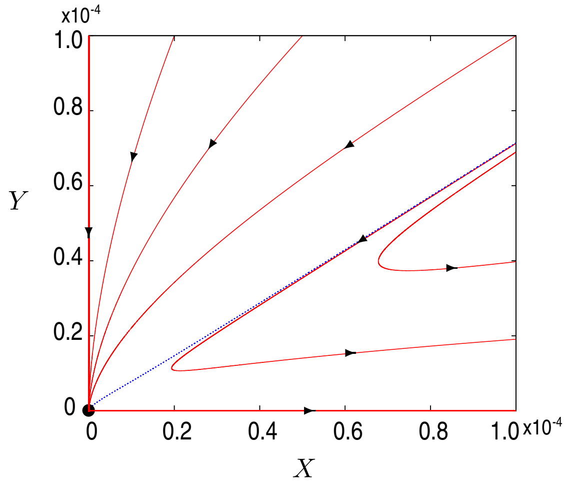

Fig. 10. Phase portrait of system B_{ii} without the Allee effect for the parameters satisfying $D < C < 1 + D < M_H < M < \frac{C}{C-D}$, where the blue radial denotes $\theta = \theta^* = \tan^{-1}(-\frac{1+D-C}{1+D-M})$.

simulations, we choose $E = 0.4$ and $D = 0.8$. For the case $C \geq D + \frac{(1-E)^2}{4} = 0.89$, we take $C = 0.95$ and $M = 0.3 < M_u = 0.57$. The simulated trajectories either converge to the stable node E_0 or to the stable node E_{3+}, as shown in Fig. 11(a).

For the case $D < C < D + \frac{(1-E)^2}{4} = 0.89$, we choose $C = 0.82$, yielding $M_u = 3.69$ and $M_H = 3.6086$. We first take $M = 3.58$ under which E_{3+} is a stable focus, with trajectories still either converging to the stable node E_0 or to the stable focus E_{3+}, as seen from Fig. 11(b). It seems that the unstable limit cycle does not exist for these parameter values. In fact, it is very difficult to identify the parameter values to obtain such unstable limit cycles. We have to search the parameter values of M very close to the Hopf critical point M_H from $M > M_H$ to $M < M_H$. For the above chosen values of E, D and C, we take four values of M, one of them is greater than M_H and the remaining three are less than M_H:

$$M = 3.61 > M_H = 3.6086, \quad \text{and}$$

$$M = 3.606, 3.59253, 3.592 < M_H = 3.6086.$$

It is easy to show that E_{3+} is an unstable focus for $M = 3.61$, but a stable focus for $M = 3.606$, 3.59253, 3.592, as expected. The simulated phase portraits for the four values of M are shown in Figs. 11(c)–11(f), respectively. It is seen that an unstable limit cycle exists at $M = 3.606$, and in fact for the above chosen values of E, D and C, unstable limit cycles exist for $3.59253 < M < M_H = 3.6086$. At $M = 3.59253$, the unstable limit cycle coincides with the unstable homoclinic loop. Then E_{3+} becomes a stable focus without any closed orbits around.

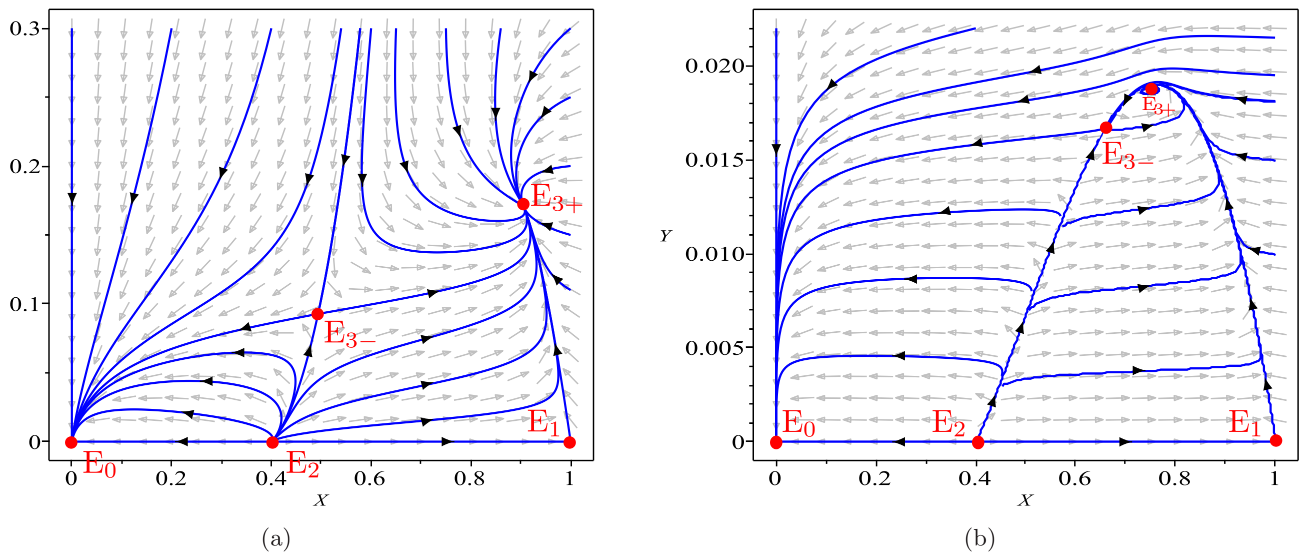

Fig. 11. Simulated phase portraits of system B_{ii} with $E = 0.4$ and $D = 0.8$: (a) $C = 0.95$ and $M = 0.3$, showing bistable equilibria E_0 and E_{3+}, with two attracting regions separated by the stable manifolds connecting to the saddle point E_{3-}; (b) $C = 0.82$ and $M = 3.58$, also showing bistable equilibria E_0 and E_{3+}, with two attracting regions separated by the stable manifolds connecting to the saddle point E_{3-}; (c) $C = 0.82$ and $M = 3.61$, showing the unstable E_{3+}; (d) $C = 0.82$ and $M = 3.606$, showing the stable E_{3+} and an unstable limit cycle; (e) $C = 0.82$ and $M = 3.59253$, showing the stable E_{3+} and the unstable homoclinic loop and (f) $C = 0.82$ and $M = 3.592$, showing the stable E_{3+}.

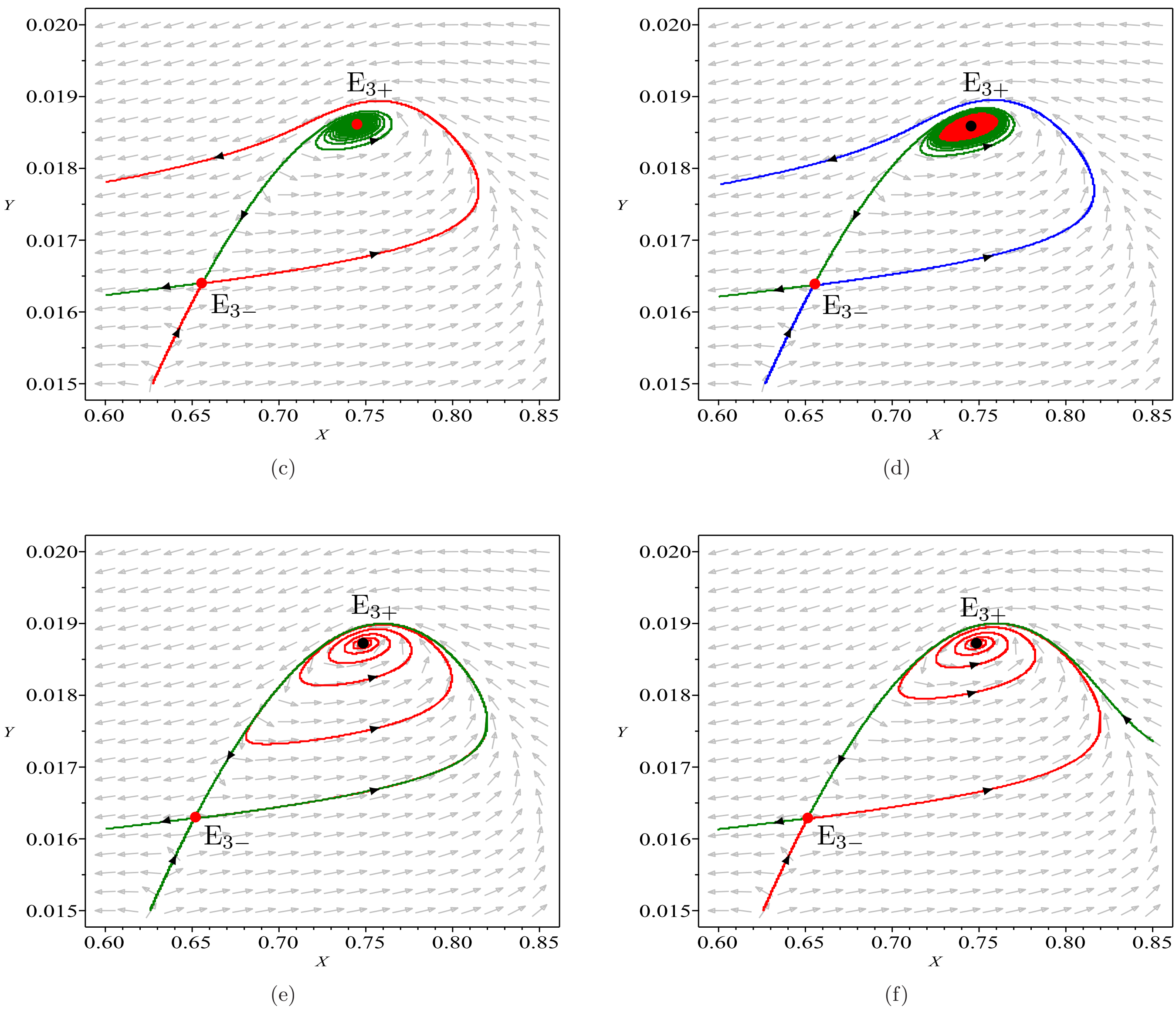

Fig. 11. (*Continued*)

Remark 5.6. It has been shown in [Xiao & Ruan, 2001] that the dynamics around the equilibrium E_0 of system B_{ii} without the Allee effect can be very complex, which may be asymptotically stable or unstable, or even including both stable and unstable sectors. However, the equilibrium E_0 of system B_{ii} with the Allee effect is always asymptotically stable. This clearly indicates that species having a strong Allee effect may affect their predation and hence extinction risk. Moreover, the B_{ii} system without the Allee effect has supercritical Hopf bifurcation generating stable limit cycles; while the B_{ii} system with the Allee effect not only changes the supercritical Hopf bifurcation to subcritical Hopf bifurcation, resulting in that the equilibrium E_{3+} becomes stable from unstable. Moreover, the unstable limit cycles exist for a very limited parameter values. To see why such a change in the Hopf bifurcation increases the stability of the system, we take a comparison of the solution trajectories shown in Fig. 9 (without the Allee effect) and in Fig. 11 (with the Allee effect). For Fig. 9 without the Allee effect, there exist values of the parameter M in an interval for which a supercritical Hopf bifurcation occurs and all trajectories converge to the stable limit cycle [see Fig. 9(a)]. Otherwise, the trajectories may converge to E_0. However, due to the complex behavior of E_0 without the Allee effect, for most parameter values, trajectories would not converge to E_0, but are oscillating. For Fig. 11 with the Allee effect, the supercritical Hopf bifurcation is changed to a subcritical Hopf bifurcation and the bifurcating limit cycle is unstable [see Fig. 11(d)], and the equilibrium E_{3+} becomes stable. In this case, all trajectories converge to the stable node E_0 (which is always stable due to the Allee effect), except those starting from initial points inside the unstable limit cycle, which converge to the stable focus E_{3+}. Since the parameter values for generating the unstable limit cycle is very limited, it clearly implies that the system becomes more stable, compared to the system without the Allee effect.

5.5. *B–T bifurcation*

The conditions for the model B_{ii} to have a B–T bifurcation are $\det(J(E_{3+})) = \mathrm{Tr}(J(E_{3+})) = 0$. It follows from (50) and (51) that the B–T bifurcation occurs when

$$C(1-E)^2 - 4M(C-D) = C - M = 0$$
$$\Rightarrow C = M = D + \frac{1}{4}(1-E)^2, \quad X_3 = \frac{1}{2}(1+E). \tag{56}$$

Obviously, it is as expected that the B–T bifurcation occurs at the turning point $M = M_{\mathrm{u}}$ at which

$$E_{3+} = E_{3-} = E_3 = \left(\frac{1}{2}(1+E), \frac{1}{8D}(1+E)(1-E)^2\right), \tag{57}$$

where the saddle-node bifurcation coincides with the Hopf bifurcation.

To analyze the B–T bifurcation, we need to find the normal form of the B–T bifurcation with unfolding. First, we want to determine the codimension of the B–T bifurcation and then to obtain the normal form with unfolding. In the following two sections, we will apply the simplest normal form (SNF) theory (e.g. see [Yu, 1999; Gazor & Yu, 2010, 2012]) to determine the codimension of the B–T bifurcation of the system (38) and the parametric simplest normal form (PSNF) theory (e.g. see [Yu & Leung, 2003; Gazor & Moazeni, 2015]) to obtain the normal form of system (38) with unfolding terms.

5.5.1. *The SNF and the codimension for the B–T bifurcation*

In order to obtain the normal form for the B–T bifurcation, we first need to determine the codimention of the system (38). We have the following theorem.

Theorem 5.7. *For system (38), when $C = M = D+\frac{1}{4}(1-E)^2$, B–T bifurcation occurs from the equilibrium solution $E_3 : (X,Y) = (\frac{1+E}{2}, \frac{(1+E)(1-E)^2}{8D})$. The codimension of the B–T bifurcation is two and no codimension higher than two can happen for the B–T bifurcation.*

Proof. Let

$$\begin{aligned} C &= D + \frac{1}{4}(1-E)^2 + \mu_1, \\ M &= D + \frac{1}{4}(1-E)^2 + \mu_2, \end{aligned} \tag{58}$$

where μ_1 and μ_2 are perturbation parameters. Thus, $(\mu_1, \mu_2) = (0,0)$ defines the B–T bifurcation point. Now, we assume $(\mu_1, \mu_2) = (0,0)$, and apply the simplest normal form theory [Yu, 1999; Gazor & Yu, 2010, 2012] to determine the codimension of system (38). To achieve this, introducing the following transformation,

$$\begin{aligned} X &= \frac{1}{2}(1+E) + \frac{D(1-E)^2}{(1-E)^2+4D}u + v, \\ Y &= \frac{1}{8D}(1+E)(1-E)^2 + \frac{(1-E)^4}{4[(1-E)^2+4D]}u, \end{aligned} \tag{59}$$

into (38), we obtain the following system:

$$\dot{u} = f_1(u,v,D,E), \quad \dot{v} = f_2(u,v,D,E), \tag{60}$$

where f_1 and f_2 are rational functions in u and v with coefficients given in terms of D and E. Then, we expand the above system around $(u,v) = (0,0)$ and apply the SNF theory [Yu, 1999; Gazor & Yu, 2012] to the expended system, with the following nonlinear transformation truncated up to second order:

$$\begin{aligned} u &= -x_1 - \frac{(1-E^2)^2 + 16DE}{4(1+E)[(1-E)^2+4D]}x_1^2, \\ v &= -x_2 - \frac{(1-E^2)^2 + 16DE}{2(1+E)[(1-E)^2+4D]}x_1x_2 \\ &\quad + \frac{8D}{(1+E)[(1-E)^2+4D]}x_2^2, \end{aligned} \tag{61}$$

introduced into (60) to obtain the SNF up to second-order terms:

$$\begin{aligned} \dot{x}_1 &= x_2 + \mathcal{O}(|(x_1,x_2)|^3), \\ \dot{x}_2 &= C_{20}x_1^2 + C_{11}x_1x_2 + \mathcal{O}(|(x_1,x_2)|^3), \end{aligned}$$

where

$$C_{20} = \frac{D^2(1+E)(1-E)^4}{2[(1-E)^2+4D]} > 0,$$
$$C_{11} = \frac{D(1+E)(1-E)^2}{(1-E)^2+4D} > 0. \tag{62}$$

Further, introducing the transformation,

$$x_1 \to x_1, \quad x_2 + \mathcal{O}(|(x_1,x_2)|^3) \to x_2,$$

into the above equations, we obtain

$$\dot{x}_1 = x_2,$$
$$\dot{x}_2 = C_{20}x_1^2 + C_{11}x_1x_2 + \mathcal{O}(|(x_1,x_2)|^3). \tag{63}$$

Since $C_{20}C_{11} \neq 0$, the codimension of the B–T bifurcation is two. ■

5.5.2. *The PSNF of the B–T bifurcation and bifurcation analysis*

In this section, we use the PSNF theory to obtain the normal forms with unfolding up to second-order terms for the codimension-two B–T bifurcation, and give a summary on the bifurcation analysis. Here, we will obtain the normal form with the unfolding terms expressed in the original system parameters.

To obtain the normal form with unfolding, we introduce the parametric transformation,

$$C = D + \frac{1}{4}(1-E)^2 + \mu_1,$$
$$M = D + \frac{1}{4}(1-E)^2 + \mu_2, \tag{64}$$

together with the change of state variables (59), into (38) to obtain

$$\dot{u} = F_1(u,v,\mu_1,\mu_2,D,E),$$
$$\dot{v} = F_2(u,v,\mu_1,\mu_2,D,E). \tag{65}$$

Then, we expand the above system around the point $(u,v,\mu_1,\mu_2) = (0,0,0,0)$ and apply the PSNF theory, with another change of state variables:

$$\begin{aligned}
u = &-\frac{2[(1-E)^2+4D]^2}{D^2(1+E)(1-E)^4}x_1\\
&+\frac{[(1-E)^2+4D]^3[(1+E)^2(1-E)^4-4(1-E)^2(1-10E+E^2)D+16(1+E)^2D^2]}{D^5(1+E)(1-E)^{10}}\beta_1\\
&-\frac{(1+E)[(1-E)^2+4D]^2}{2(1-E)^4D^2}\beta_2+\frac{2[(1-E)^2+8D][(1-E)^2+4D]^2}{D^3(1+E)(1-E)^6}\beta_2x_1\\
&-\frac{[(1-E^2)^2+16DE][(1-E)^2+4D]^3}{D^4(1+E)^3(1-E)^8}x_1^2\\
&-\frac{[(1+E)^2(1-E)^4+4(1-E)^2(1+6E+E^2)D+16(3-2E+3E^2)D^2][(1-E)^2+4D]^3}{D^5(1+E)^3(1-E)^{10}}x_1x_2\\
&-\left\{\frac{[(1-E)^2+8D][(1-E)^2+4D]^3[(1+E)^2(1-E)^4+4(1-E)^2(1+6E+E^2)D]}{4(1-E)^{12}(1+E)^3D^6}\right.\\
&\left.+\frac{16D^2[(1-E)^2+8D][(1-E)^2+4D]^3(3-2E+3E^2)}{4(1-E)^{12}(1+E)^3D^6}\right\}x_2^2,\\
v = &-\frac{2[(1-E)^2+4D]^2}{D^2(1+E)(1-E)^4}x_2\\
&-\frac{[(1+E)^2(1-E)^4+4(1-E)^2(1+6E+E^2)D+16(3-2E+3E^2)D^2][(1-E)^2+4D]^2}{8D^4(1+E)(1-E)^8}\beta_1\\
&+\frac{(1+E)[(1-E)^2+4D]}{2D(1-E)^2}\beta_2-\frac{2[(1-E)^2+4D]^2}{D^2(1+E)(1-E)^4}\beta_2x_1
\end{aligned}$$

$$- \frac{2[(1-E^2)^2+16DE][(1-E)^2+4D]^3}{D^4(1+E)^3(1-E)^8}x_1x_2$$
$$- \frac{[(1+E)^2(1-E)^4+4(1-E)^2(1+6E+E^2)D-16(E^2-6E+1)D^2][(1-E)^2+4D]^3}{2D^5(1+E)^3(1-E)^{10}}x_2^2, \tag{66}$$

as well as the parametric transformation:

$$\begin{aligned}
\mu_1 = {} & -\frac{[(1+E)^2(1-E)^4+4(1-E)^2(1+6E+E^2)D+16(3-2E+3E^2)D^2][(1-E)^2+4D]^2}{16D^4(1+E)^2(1-E)^6}\beta_1 \\
& - \frac{(1-E)^2+4D}{4D}\beta_2 + \frac{[(1-E)^2+4D]^4}{2D^4(1+E)^2(1-E)^6}\beta_1\beta_2 \\
& + \frac{[(1+E)^2(1-E)^4+4(1-E)^2(1+6E+E^2)D+16(3-2E+3E^2)D^2][(1-E)^2+4D]^5}{8D^7(1+E)^4(1-E)^{12}}\beta_1^2, \\
\mu_2 = {} & -\frac{[(1+E)^2(1-E)^4-4(1-E)^2(3-14lE+3E^2)D-16(E^2-6E+1)D^2][(1-E)^2+4D]^2}{4D^3(1-E)^8(1+E)^2}\beta_1 \\
& + \frac{(1-E)^2+4D}{(1-E)^2}\beta_2 + \left\{\frac{[(1+E)^4(1-E)^8-16(E^2-6E+1)(1+E)^2(1-E)^6D][(1-E)^2+4D]^4}{16D^7(1+E)^4(1-E)^{16}}\right. \\
& - \frac{[(5E^4+20E^3-146E^2+20E+5)(1-E)^2+8D(E^4+20E^3-74E^2+20E+1)][(1-E)^2+4D]^4}{D^5(1+E)^4(1-E)^{14}} \\
& \left. - \frac{16(5E^2-14E+5)(1+E)^2[(1-E)^2+4D]^4}{D^3(1+E)^4(1-E)^{16}}\right\}\beta_1^2 \\
& - \frac{[(1+E)^2(1-E)^4+32E(1-E)^2D+64ED^2][(1-E)^2+4D]^3}{2D^4(1+E)^2(1-E)^{10}}\beta_1\beta_2 + \frac{[(1-E)^2+4D]^2}{D(1-E)^4}\beta_2^2
\end{aligned} \tag{67}$$

to obtain the standard normal form with unfolding:

$$\begin{aligned}
\dot{x}_1 &= x_2 + \mathcal{O}(|(x_1,x_2,\mu_1,\mu_2)|^3), \\
\dot{x}_2 &= \beta_1 + \beta_2 x_2 + x_1^2 + \frac{2[(1-E)^2+4D]}{D(1-E)^2}x_1x_2 \\
&\quad + \mathcal{O}(|(x_1,x_2,\mu_1,\mu_2)|^3).
\end{aligned}$$

Finally, introducing the transformation

$$x_1 \to x_1, \quad x_2 + \mathcal{O}(|(x_1,x_2,\mu_1,\mu_2)|^3) \to x_2,$$

into the above system yields the normal form with unfolding up to second-order terms:

$$\begin{aligned}
\dot{x}_1 &= x_2, \\
\dot{x}_2 &= \beta_1 + \beta_2 x_2 + x_1^2 + \frac{2[(1-E)^2+4D]}{D(1-E)^2}x_1x_2 \\
&\quad + \mathcal{O}(|(x_1,x_2,\beta_1,\beta_2)|^3),
\end{aligned} \tag{68}$$

where we keep the parameters D and E in the coefficient in order to see how the original system parameters affect the bifurcation behavior of the system.

Now, we use the normal form (68) to analyze the codimension-two B–T bifurcation. Note that the normal form (68) is in the standard form given in [Guckenheimer & Holmes, 1993]. Thus, we follow the approach described in [Guckenheimer & Holmes, 1993] to obtain the following result.

Theorem 5.8. *For the* $\mathrm{B_{ii}}$ *system (38), codimension-two B–T bifurcation occurs from the equilibrium*

$$\mathrm{E}_3 : (X,Y) = \left(\frac{1+E}{2}, \frac{(1+E)(1-E)^2}{8D}\right)$$

when

$$C = M = D + \frac{1}{4}(1-E)^2.$$

Moreover, three local bifurcations with the representations of the bifurcation curves are given below.

(1) *Saddle-node bifurcation occurs from the bifurcation curve*:

$$\mathrm{SN} = \{(\beta_1, \beta_2) \,|\, \beta_1 = 0\}.$$

(2) *Hopf bifurcations occur from the bifurcation curve*:

$$\mathrm{H} = \left\{ (\beta_1, \beta_2) \,\middle|\, \beta_1 = -\left[\frac{D(1-E)^2}{2((1-E)^2 + 4D)}\right]^2 \beta_2^2, \beta_2 > 0 \right\}, \quad \textit{subcritical.}$$

(3) *Homoclinic orbits occur from the bifurcation curve*:

$$\mathrm{HL} = \left\{ (\beta_1, \beta_2) \,\middle|\, \beta_1 = -\frac{49}{25}\left[\frac{D(1-E)^2}{2((1-E)^2 + 4D)}\right]^2 \beta_2^2, \beta_2 > 0 \right\}, \quad \textit{unstable.}$$

The bifurcation diagram for the B–T bifurcation is shown in Fig. 12. Note that the Hopf bifurcation is subcritical, which agrees with the Hopf bifurcation analysis given in the previous section. In addition, it is seen that variations on the parameters do not change the qualitative property of bifurcations since the coefficient $[\frac{D(1-E)^2}{2((1-E)^2+4D)}]^2$ keeps its sign unchanged. Moreover, it is easy to see that

$$\left[\frac{D(1-E)^2}{2((1-E)^2 + 4D)}\right]^2 = \left[\frac{1}{\dfrac{8}{(1-E)^2} + \dfrac{2}{D}}\right]^2 < \frac{(1-E)^4}{64},$$

indicating that the Allee effect has a great impact on the quantitative bifurcation property when D is not too small.

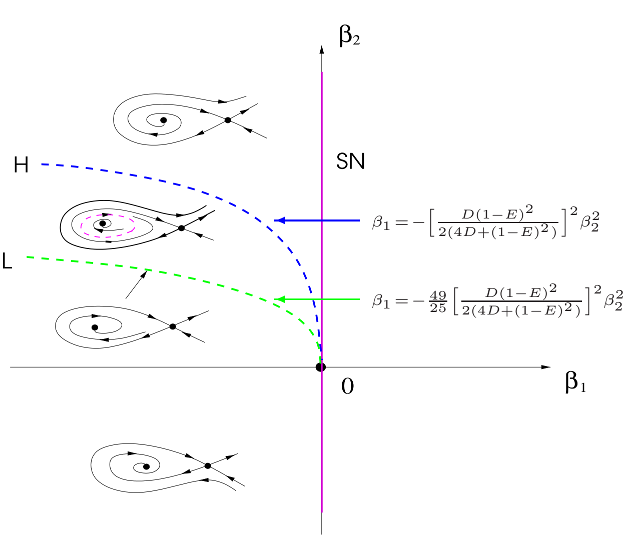

Fig. 12. B–T bifurcation sets and phase portraits of system (68).

The formulas for bifurcation curves, given in Theorem 5.8, can be expressed in terms of the original perturbation parameters μ_1 and μ_2 via (67). In the following, we discuss how to simulate the dynamical phenomena in the above B–T Bifurcation using the original system (38), in particular for the Hopf bifurcation and the homoclinic loop bifurcation. With (58),

$$C = D + \frac{1}{4}(1-E)^2 + \mu_1,$$

$$M = D + \frac{1}{4}(1-E)^2 + \mu_2,$$

the condition $D < C < D + \frac{1}{4}(1-E)^2$ yields

$$\mu_1 > -\frac{1}{4}(1-E)^2.$$

Further, to have solutions $\mathrm{E}_{3\pm}$, we need

$$M < M_u = \frac{C(1-E)^2}{4(C-D)} \Rightarrow \mu_2 < \frac{D[-4 + (1-E)^2]}{4\mu_2 + (1-E)^2}.$$

For simulation, we again take $E = 0.4$, $D = 0.8$ and thus obtain the critical value $C = M = 0.89$ at which the positive equilibrium becomes $\mathrm{E}_{3+} = (0.7, 0.07875)$. Thus, $\mu_1 > -0.09$. For simplicity, choose $\mu_1 = -0.04$. Then, $\mu_2 < -\frac{0.8\mu_1}{\mu_1+0.09} = 0.64$. We vary μ_2 as

$$\mu_2 = 0.63, 0.628, 0.62255, 0.62.$$

It is easy to show that for $\mu_2 = 0.63$, E_{3+} is an unstable focus, while a stable focus for $\mu_2 = 0.628, 0.62255$ and 0.62. Moreover, an unstable limit cycle exists for $\mu_2 = 0.628$, the unstable limit cycle coincides with the homoclinic loop at $\mu_2 = 0.62255$. When $\mu_2 < 0.62255$, the homoclinic loop is broken and E_{3+} is a stable focus. The simulated phase

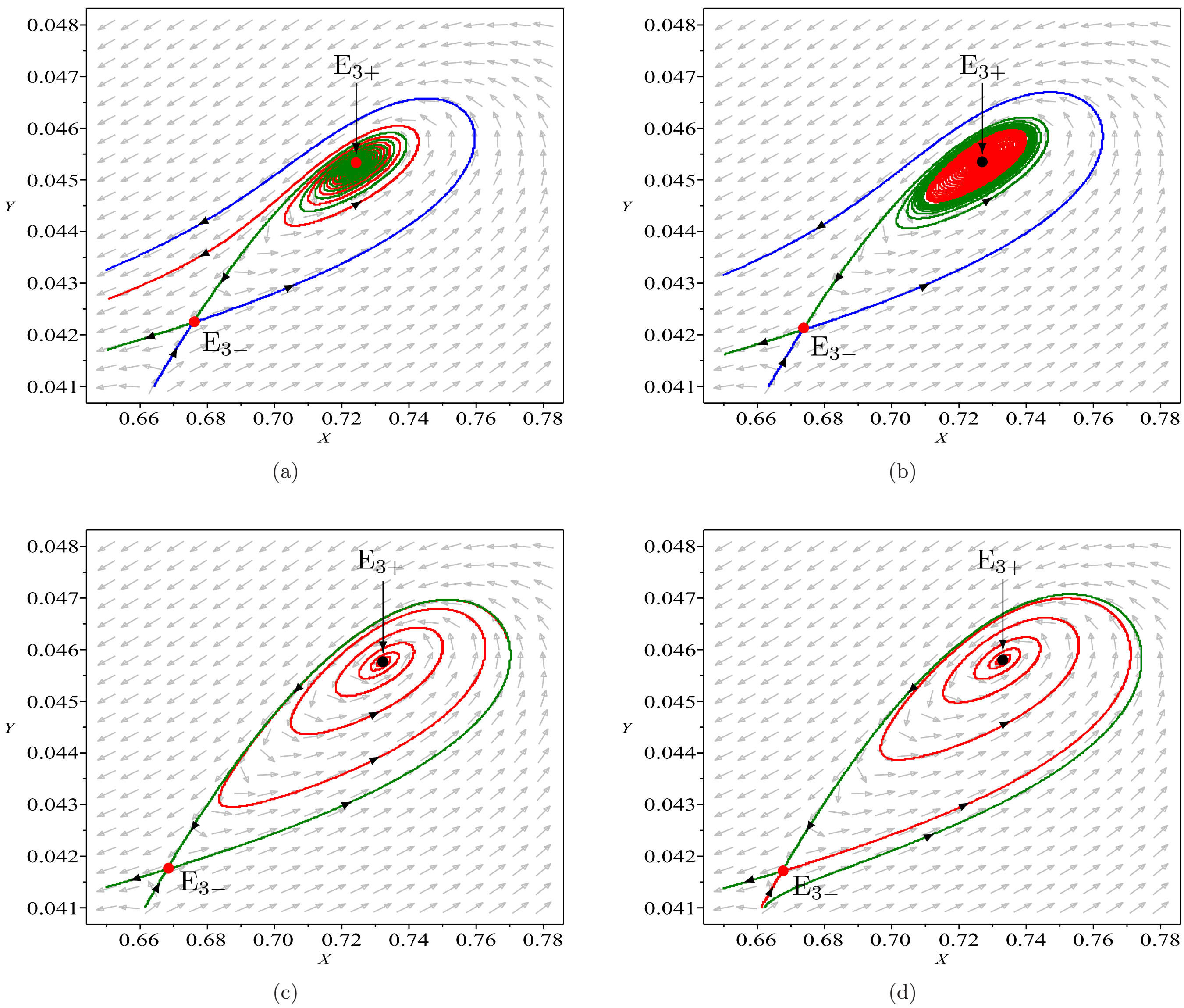

Fig. 13. Simulated phase portraits of system B_{ii} for B–T bifurcation with $E = 0.4$, $D = 0.8$ and $\mu_1 = -0.04$: (a) $\mu_2 = 0.63$, showing the unstable focus E_{3+}; (b) $\mu_2 = 0.628$, showing the stable focus E_{3+} and an unstable limit cycle; (c) $\mu_2 = 0.62255$, showing the stable focus E_{3+} and the unstable homoclinic loop and (d) $\mu_2 = 0.62$, showing the stable focus E_{3+}.

portraits for the four cases are shown in Figs. 13(a)–13(d), respectively, which correspond to the four phase portraits in the B–T bifurcation diagram (see Fig. 12) from the top to the bottom. However, it should be noted that due to the transformation (66), the simulated phase portraits in the original X- and Y-axes have the saddle point E_{3-} on the left side of the focus E_{3+} (see Fig. 13), while the B–T bifurcation diagram (see Fig. 12) has the saddle point on the right side of the focus point.

It should be pointed out that although the four phase portraits in Figs. 13(a)–13(d) are similar to those four phase portraits in Figs. 11(c)–11(f), they are quite different since the former can be only obtained near the B–T bifurcation point, while the later can be found near any Hopf bifurcation point.

6. Conclusion

In this paper, we have studied four predator–prey models and paid particular attention on the Allee effect. It has been shown that strong Allee effect has great influence on the dynamics of the system, in particular on stability and bifurcations. Compared to the systems without the Allee effect, when the density of prey population is low, the species having a strong Allee effect are vulnerable to extinction due to predation. In general, the Allee effect makes the dynamics of the systems more complicated. Especially, for the B_{ii} model, the Allee effect not only completely changes the stability of the equilibrium at the origin, but also changes the supercritical Hopf bifurcation to subcritical Hopf bifurcation with very limited parameter values for the bifurcating unstable limit cycles. Also this model with the Allee effect yields Bogdanov–Takens bifurcation, inducing more complex bifurcation behaviors. This study shows that including the Allee effect in predator–prey systems is necessary in order to have a more realistic analysis. Future works will focus on more complex systems A_{iii}, B_{iii}, C_i, C_{ii} and C_{iii}.

Acknowledgment

This research was partially supported by the Natural Sciences and Engineering Research Council of Canada, No. R2686A02.

References

Abrams, P. A. & Ginzburg, L. R. [2000] "The nature of predation: Prey dependent, ratio dependent or neither?" *Trends in Ecol. Evol.* **15**, 337–341.

Allee, W. C. [1932] *Animal Aggregations*: *A Study in General Sociology* (University of Chicago Press, Chicago).

Arditi, R. & Ginzburg, L. R. [1989] "Coupling in predator–prey dynamics: Ratio dependence," *J. Theor. Biol.* **139**, 311–326.

Bazykin, A. D. [1988] *Nonlinear Dynamics of Interaction Populations*, World Sci. Ser. Nonlinear Sci. Ser. A., Vol. 11. (World Scientific, Singapore).

Dumortier, F., Roussarie, R. & Sotomayor, J. [1987] "Generic 3-parameter families of vector fields on the plane, unfolding a singularity with nilpotent linear part. The cusp case of codimension 3," *Erg. Th. Dyn. Syst.* **7**, 375–413.

Freedman, H. I. [1980] *Deterministic Mathematical Models in Population Ecology* (Marcel Dekker, NY).

Gause, G. G. [1969] *The Struggle for Existence* (Hafner Publishing Company, NY).

Gazor, M. & Yu, P. [2010] "Formal decomposition method and parametric normal form," *Int. J. Bifurcation and Chaos* **20**, 3487–3415.

Gazor, M. & Yu, P. [2012] "Spectral sequences and parametric normal forms," *J. Diff. Eqs.* **252**, 1003–1030.

Gazor, M. & Moazeni, M. [2015] "Parametric normal forms for Bogdanov–Takens singularity; the generalized saddle-node case," *Discr. Contin. Dyn. Syst.* **35**, 205–224.

Guckenheimer, J. & Holmes, P. [1993] *Nonlinear Oscillations*, *Dynamical Systems*, *and Bifurcations of Vector Fields*, 4th edition (Springer-Verlag, NY).

Holling, C. S. [1959] "Some characteristics of simple types of predation and parasitism," *The Canad. Entomol.* **91**, 385–398.

Holling, C. S. [1965] "The functional response of predators to prey density and its role in mimiery and population regulation," *Mem. Entomol. Soc. Canada* **97**, 5–60.

Hsu, S. B., Hwang, T. W. & Kuang, Y. [2001] "Global analysis of the Michaelis–Menten type ratio-dependent predator–prey system," *J. Math. Biol.* **42**, 489–506.

Huang, J., Ruan, S. & Song, J. [2014] "Bifurcations in a predator–prey system of Leslie type with generalized Holling type III functional response," *J. Diff. Eqs.* **257**, 1721–1752.

Jiang, J. & Yu, P. [2017] "Multistable phenomena involving equilibria and periodic motions in predator–prey systems," *Int. J. Bifurcation and Chaos* **27**, 1750043-1–28.

Jiang, J., Zhang, W. & Yu, P. [2020] "Tristable phenomenon in a predator–prey system arsing from multiple limit cycles bifurcation," *Int. J. Bifurcation and Chaos* **30**, 2050129-1–23.

Kuang, Y. & Beretta, E. [1998] "Global qualitative analysis of a ratio-dependent predator–prey system," *J. Math. Biol.* **36**, 389–406.

Kuang, Y. [1999] "Rich dynamics of Gause-type ratio-dependent predator–prey systems," *Fields Inst. Commun.* **21**, 325–337.

Li, B. & Kuang, Y. [2007] "Heteroclinic bifurcation in the Michaelis–Menten-type ratio-dependent predator–prey system," *SIAM J. Appl. Math.* **67**, 1453–1464.

Li, C., Li, J. & Ma, Z. [2015] "Codimension 3 B-T bifurcations in an epidemic model with a nonlinear incidence," *Discr. Contin. Dyn. Syst. Ser. S* **20**, 1107–1116.

Lotka, A. J. [1925] *Elements of Physical Biology* (Williams and Wilkins, Baltimore).

Ma, Z., Li, W., Zhao, Y., Wang, W., Zhang, H. & Li, Z. [2009] "Review effects of prey refuges on a predator–prey model with a class of functional responses: The role of refuges," *Math. Biosci.* **218**, 73–79.

Murray, J. D. [2002] *Mathematical Biology* (*II*), (Springer-Verlag, Heidelberg).

Rana, S., Bhowmick, A. R. & Bhattacharya, S. [2014] "Impact of prey refuge on a discrete time predator–prey system with Allee effect," *Int. J. Bifurcation and Chaos* **24**, 1450106-1–19.

Verma, V. & Misra, A. K. [2018] "Modeling the effect of prey refuge on a ratio-dependent predator–prey system with the Allee effect," *Bull. Math. Biol.* **80**, 626–656.

Volterra, V. [1926] "Fluctuations in the abundance of species considered mathematically," *Nature* **118**, 558–560.

Xiao, D. & Ruan, S. [2001] "Global dynamics of a ratio-dependent predator–prey system," *J. Math. Biol.* **43**, 268–290.

Xiao, D., Li, W. & Han, M. [2006] "Dynamics in a ratio-dependent predator prey model with predator harvesting," *J. Math. Anal. Appl.* **324**, 14–29.

Yu, P. [1998] "Computation of normal forms via a perturbation technique," *J. Sound Vib.* **211**, 19–38.

Yu, P. [1999] "Simplest normal forms of Hopf and generalized Hopf bifurcations, " *Int. J. Bifurcation and Chaos* **9**, 1917–1939.

Yu, P. & Leung, A. Y. L. [2003] "The simplest normal form of Hopf bifurcation," *Nonlinearity* **16**, 277–300.

Yu, P., Zhang, W. & Wahl, L. W. [2016] "Dynamical analysis and simulation of a 2-dimensional disease model with convex incidence," *Commun. Nonlin. Sci. Numer. Simulat.* **37**, 163–192.

Yu, P. & Zhang, W. [2019] "Complex dynamics in a unified SIR and HIV disease model: A bifurcation theory approach," *J. Nonlin. Sci.* **29**, 2447–2500.

Zeng, B., Deng, S. & Yu, P. [2020] "Analysis on recurrence behavior in oscillating networks of biologically relevant organic reactions," *Discr. Contin. Dyn. Syst. Ser. S* **13**, 3253–3269.

Zhang, Z., Ding, T., Huang, W. & Dong, Z. [1991] *Qualitative Theory of Differential Equations*. Translations of Mathematical Monographs, Vol. 101 (Amer. Math. Soc., Providence).

Zhang, W., Wahl, L. W. & Yu, P. [2013] "Conditions for transient viremia in deterministic in-host models: Viral blips need no exogenous trigger," *SIAM J. Appl. Math.* **73**, 853–881.

Zhang, W., Wahl, L. W. & Yu, P. [2014] "Viral blips may not need a trigger: How transient viremia can arise in deterministic in-host models," *SIAM Rev.* **56**, 127–155.